The Meteoritical Society

Meteoritics & Planetary Science 52, Nr 11, 2391–2410 (2017)
doi: 10.1111/maps.12953

Basalt–trachybasalt samples in Gale Crater, Mars

Peter H. EDWARDS[1], John C. BRIDGES[1*], Roger WIENS[2], Ryan ANDERSON[3], Darby DYAR[4], Martin FISK[5], Lucy THOMPSON[6], Patrick GASDA[2], Justin FILIBERTO[7], Susanne P. SCHWENZER[8], Diana BLANEY[9], and Ian HUTCHINSON[1]

[1]Department of Physics and Astronomy, Leicester Institute for Space and Earth Observation, University of Leicester, Leicester LE1 7RH, UK
[2]Los Alamos National Lab, Los Alamos, New Mexico 87545, USA
[3]USGS Astrogeology Science Center, Flagstaff, Arizona 86001, USA
[4]Mineral Spectroscopy Laboratory, Mount Holyoke College, South Hadley, Massachusetts 01075, USA
[5]College of Earth, Ocean, and Atmospheric Sciences, Oregon State University, Corvallis, Oregon 97331, USA
[6]Planetary and Space Science Centre, University of New Brunswick, Fredericton, New Brunswick E3B 5A3, Canada
[7]Geology Department, Southern Illinois University, 1259 Lincoln Drive, Carbondale, Illinois 62901, USA
[8]Department of Environment, Earth and Ecosystems, The Open University, Milton Keynes MK7 6AA, UK
[9]Jet Propulsion Laboratory, Pasadena, California 91109, USA
[*]Corresponding author. E-mail: j.bridges@le.ac.uk

(Received 15 June 2016; revision accepted 25 July 2017)

Abstract–The ChemCam instrument on the Mars Science Laboratory (MSL) rover, Curiosity, observed numerous igneous float rocks and conglomerate clasts, reported previously. A new statistical analysis of single-laser-shot spectra of igneous targets observed by ChemCam shows a strong peak at ~55 wt% SiO_2 and 6 wt% total alkalis, with a minor secondary maximum at 47–51 wt% SiO_2 and lower alkali content. The centers of these distributions, together with the rock textures, indicate that many of the ChemCam igneous targets are trachybasalts, Mg# = 27 but with a secondary concentration of basaltic material, with a focus of compositions around Mg# = 54. We suggest that all of these igneous rocks resulted from low-pressure, olivine-dominated fractionation of Adirondack (MER) class-type basalt compositions. This magmatism has subalkaline, tholeiitic affinities. The similarity of the basalt endmember to much of the Gale sediment compositions in the first 1000 sols of the MSL mission suggests that this type of Fe-rich, relatively low-Mg#, olivine tholeiite is the dominant constituent of the Gale catchment that is the source material for the fine-grained sediments in Gale. The similarity to many Gusev igneous compositions suggests that it is a major constituent of ancient Martian magmas, and distinct from the shergottite parental melts thought to be associated with Tharsis and the Northern Lowlands. The Gale Crater catchment sampled a mixture of this tholeiitic basalt along with alkaline igneous material, together giving some analogies to terrestrial intraplate magmatic provinces.

INTRODUCTION

Since landing on the surface of Mars on August 6, 2012, NASA's Mars Science Laboratory (MSL) rover, Curiosity, has analyzed a wide variety of geological targets ranging from sedimentary outcrops and soils to a large number of float rocks. Over the first 1000 sols of its mission, Curiosity traveled 10.6 km. Many of the float rocks it encountered are of igneous origin emplaced through fluvial and also perhaps impact processes postdating the formation of Gale Crater itself in the early Hesperian (Milliken et al. 2010). In this paper, we use data from the ChemCam instrument on MSL, which has now taken over 400,000 spectra over

the course of the mission to date (Maurice et al. 2016), in order to determine the compositions of the igneous rocks and compare them to shergottite meteorites and igneous rocks from previous rover missions, and to provide new insights about Martian magmatism. The large amount of data enables representative, average compositions to be calculated for each of the different types of Gale igneous rock. In this paper, we take a "large-data" approach, complementary to observations of individual igneous rocks (Sautter et al. 2014, 2015; Cousin et al. 2017; Mangold et al. 2017).

Before the MSL mission, knowledge of igneous rocks from Mars relied on the study of Martian meteorites (e.g., McSween and Treiman 1998); alpha particle X-ray spectrometer (APXS) in situ analyses from previous landers, in particular the Mars Exploration Rovers (MER), Spirit and Opportunity (e.g., Squyres et al. 2004); and surface mineralogy and derived chemistry from orbiter analyses (e.g., Poulet et al. 2009). The Martian crust is dominated by basaltic compositions and mineralogy (e.g., Bandfield 2000; Dunn et al. 2007; Koeppen and Hamilton 2008; Poulet et al. 2009; Taylor et al. 2010; Rogers and Hamilton 2015), with only localized possible evolved rocks (e.g., Bandfield 2004; Carter and Poulet 2013; Wray et al. 2013; Sautter et al. 2015). Similarly, the shergottite Martian meteorites are basaltic in nature (e.g., Bridges and Warren 2006; McSween et al. 2015; Treiman and Filiberto 2015), with limited evidence for evolved magma compositions in melt inclusions and clasts (e.g., Ikeda 2005; Nekvasil et al. 2007; Santos et al. 2015).

Specifically, the most abundant type of Martian meteorite, the shergottites, show a very restricted range in chemistry and are relatively alkali-poor, Fe-rich, undifferentiated basaltic rocks. They are dominated by pyroxene with shocked plagioclase and variable amounts of olivine. They represent a mixture of cumulates and melts (e.g., Musselwhite et al. 2005; Bridges and Warren 2006; McSween et al. 2009, 2015; Filiberto and Dasgupta 2011, 2015; Gross et al. 2011; Treiman and Filiberto 2015). The meteorites have a range of compositions close to near-primary magmas and partially evolved magmas (e.g., Musselwhite et al. 2005; Shearer et al. 2008, 2013; Filiberto and Dasgupta 2011, 2015; Gross et al. 2011; Papike et al. 2013; McSween et al. 2015; Treiman and Filiberto 2015). Mantle source regions for the basalt generation were Fe- and relatively total alkali-rich and Al-poor compared to the Earth's mantle basalt source (Stolper and McSween 1979; Dreibus and Wänke 1985; Taylor 2013).

However, the MER APXS analyses of igneous rocks at both Gusev Crater and Meridiani Planum revealed a wider range in chemistry than in the meteorite collection, showing the Fe-rich basaltic signature, but also with some more alkali-rich magmatic compositions (McSween and Ruff 2006; Ming et al. 2008; Usui et al. 2008; McSween et al. 2008, 2009; and also shock features (Zipfel et al. 2011). Opportunity only analyzed one relatively unaltered basaltic rock—Bounce Rock—which has a similar bulk chemistry and mineralogy to Martian meteorites Elephant Moraine (EET) 79001 lithology B and Queen Alexandra Range (QUE) 94201 (Zipfel et al. 2011). Spirit analyzed a number of basaltic rocks (e.g., McSween and Ruff 2006; McSween et al. 2008), providing significant constraints on the source region of these basalts, and the evolution of Martian magmas and crust at Gusev Crater (e.g., McCubbin et al. 2008; Schmidt and McCoy 2010; Filiberto and Dasgupta 2011, 2015; Schmidt et al. 2013). Spirit landed on a possible basaltic lava flow, the Adirondack class of picritic rocks was identified within the plains, and it was not until it reached the Columbia Hills that it analyzed a diverse suite of rocks including ultramafic cumulates, silica-saturated, relatively alkali-rich (alkalic) basalts, and a pyroclastic deposit (e.g., McSween and Ruff 2006; Squyres et al. 2007; Ming et al. 2008; Usui et al. 2008; McSween et al. 2009). The Gusev samples analyzed by the Spirit APXS included a subset—the Wishstone Class—which have moderately alkaline-rich compositions (though not silica-undersaturated), with a pyroclastic rock and two lava flow or intrusive samples (McSween and Ruff 2006). These were considered to have formed by fractional crystallization of primitive, basaltic magma, similar to olivine-rich basalts also seen at Gusev. These basalts are the Adirondack class, and we will also consider this basalt composition in order to interpret the Gale data.

Analyses of float rocks early in the MSL mission identified some alkaline-rich samples of uncertain provenance—either igneous or sedimentary in origin. Notably, the float rock Jake_M had APXS analyses that showed Na_2O+K_2O contents of ~9 wt%, and is alkaline in nature with >15% normative nepheline, making it compositionally similar to terrestrial mugearites (Stolper et al. 2013) though its igneous or sedimentary origin is generally considered uncertain. Schmidt et al. (2014) used APXS analyses from Curiosity to highlight the occurrence of alkali (in particular K_2O) enrichments in some of the basaltic Gale sediments suggesting that the source region contained alkali-rich minerals. Much stronger K enrichments, with some higher than 5 wt% K_2O, have been found in all sediments in the Kimberley region (Le Deit et al. 2016). The CheMin X-ray diffraction instrument showed that these compositions are due to

the presence of alkali-rich feldspars (Treiman et al. 2016). Treiman and Filiberto (2015) showed that Gale Crater K enrichments are similar to the parental magmas of the nakhlite meteorites. However, the proportion of alkali-rich material within the Gale catchment, compared to subalkaline basaltic material for instance, has been unclear and CheMin XRD analyses of Rocknest and Namib eolian material (Achilles et al. 2016) do not have an alkaline mineralogy.

Sautter et al. (2014, 2015) also used ChemCam compositional analyses and Remote Micro-Imager (RMI) data from the first part of the mission to highlight and classify the occurrence of both feldspar-rich, extrusive igneous rocks and dark, basaltic rocks within the float samples and Hottah facies outcrop conglomerate clasts (Williams et al. 2013). Sautter et al. first identified that the feldspar-rich lithologies were extrusive and suggested they might be ancient crust analogous to the lunar highlands transported from the crater rim, incorporated into the coarse gravel, or conglomerate clasts.

The MSL ChemCam, laser-induced breakdown spectroscopy (LIBS) data, with a recalibration (Clegg et al. 2016), provide a new opportunity to study igneous rocks on the surface of Mars and determine their origin within the framework of what we have learnt about the differentiation of basalt and related rocks on Earth. Some of the questions we address include the likely crystal fractionation controls on the differentiated igneous samples in Gale, the specific magmatic differentiation series (e.g., alkaline or tholeiitic), the relative importance of different igneous compositions preserved in Gale, and their similarities or differences to MER and shergottite basalts. In this work, we used a statistical approach, rather than focusing on individual targets, in an attempt to understand how the bulk of igneous samples observed in Gale relates to previous observations.

ALKALINE BASALT NOMENCLATURE

Basalts and related rocks with moderately elevated alkali contents, which are also silica-saturated, are often described as alkalic or mildly alkaline in the recent literature (e.g., McSween and Ruff 2006; Nekvasil et al. 2007). Some ambiguity for basaltic compositions can arise through the use of 2-D total alkalis versus SiO_2 plots with the alkaline/subalkaline divide of Irvine and Baragar (1971). As shown by Delong and Hoffman (1975), some rocks with tholeiitic mineralogy fall in the alkali basalt field of an alkali/silica 2-D plot, and this is an artifact of the projection from the 3-D basalt tetrahedron implicit in making the plot. To avoid this ambiguity, and in particular because discussion of tholeiitic affinities is a relevant issue for the Gale samples in this paper, here we refer to alkaline basalts as those with silica-undersaturated, feldspathoid normative compositions, and others which are hypersthene normative and silica-saturated as being subalkaline, or having moderately elevated alkali contents.

CHEMCAM AND LASER-INDUCED BREAKDOWN SPECTROSCOPY

The ChemCam instrument on MSL is the first LIBS instrument to be deployed on a planetary exploration mission. The physical principle underlying the LIBS technique implemented by ChemCam is that of atomic emission: a high-powered pulsed laser is used to ablate a target area, causing a few nanograms of material to break down and form a plasma. This energy excites the electrons, raising them from their base energy levels to higher ones. When they return to their original energy level, they release photons with discrete wavelengths corresponding to atomic line emissions, characteristic of the elements present within the sample (Cremers and Radziemski 2006). ChemCam incorporates both a LIBS instrument and a Remote Micro-Imager (RMI), which both use a telescope within ChemCam's mast unit; the LIBS also uses three spectrometers housed inside the rover body. The laser has a NIR wavelength of 1067 nm (Cremers and Radziemski 2006; Maurice et al. 2012; Wiens et al. 2012).

ChemCam is capable of remotely analyzing targets up to 7 m away. Each LIBS spectrum is recorded by three CCDs. Each of them examines a different range of wavelengths of light from the target source: one samples ultraviolet (UV) light from 240 to 340 nm, one concentrates on 380–470 nm in the blue–violet (VIO) range, and the final spectrometer focuses on the visible and near-infrared (VNIR) spectral range of 470–900 nm. The three-spectrometer design provides the necessary resolution required to distinguish peaks; particularly those that are closer together at the lower wavelength end of the spectrum. LIBS requires a full width at half maximum (FWHM) resolution of <0.2 nm in UV and 0.65 nm in the VNIR range. Each of these spectrometers has a Czerny-Turner design (Wiens et al. 2012). Figure 1 shows typical LIBS spectra of three ChemCam targets.

Typically, 30–50 spectra (one spectrum is produced with each single-laser pulse) are recorded from each single point on the Mars surface. Several points are observed per target in a raster pattern of, e.g., 3×3 points or linear formations, e.g., 5×1 points on a single target. The individual observational footprint for

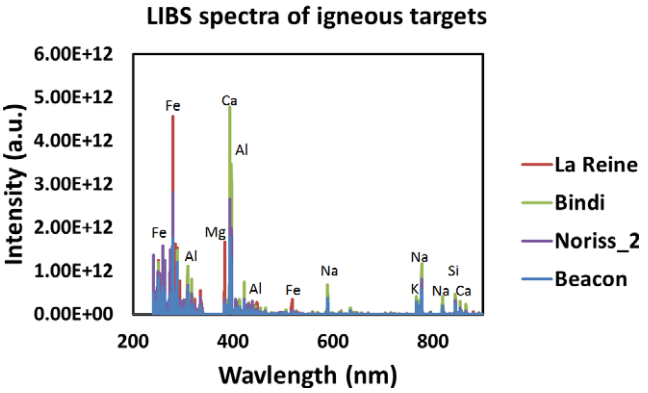

Fig. 1. The unnormalized LIBS spectra from single shot at an observation point from each of four ChemCam targets, La Reine, Bindi, Noriss_2, and Beacon. Each spectra shown here is the 10th shot of the first observation point for each target. Based on all the observation points from these targets and from imaging, Bindi and Noriss_2 are rich in feldspars (i.e., trachybasalts), while La Reine and Beacon are much richer in mafic minerals—assumed to be dominantly pyroxene. The peaks produced by the elemental line emissions are visible.

each point varies slightly in size depending on the distance from the Mast Unit, but will usually be 350–550 μm (Maurice et al. 2012, 2016). Therefore, ChemCam acts as a microprobe (Wiens and Maurice 2015) with the small diameter of laser shots on the surface, sometimes allowing characterization of individual mineral grains (Gasda et al. 2016; Cousin et al. 2017).

After the laser has fired its pulses, a dark frame is taken and this can then be subtracted from the other spectra. The data are also preprocessed to remove the Bremsstrahlung continuum and normalize the total emission of the spectrum (Wiens et al. 2013). The sequence for ChemCam data processing includes subtraction of dark spectrum, denoising, continuum removal, wavelength calibration, multiplication times the instrument response function (IRF), conversion to radiance units, and normalization (as needed), followed by masking (to remove regions of high noise in the IRF) in that order. Data are also corrected for differences in instrument response between the flight model on Mars and the laboratory spectrometers used for calibration. Therefore, select regions were masked out of the quantitative analysis models, including the 240.8–246.6, 338.5–340.8, 382.138–387.9, 473.2–492.427, and 849–905.6 nm regions. Detailed descriptions of these methods and the sample suite used for calibration are given in Wiens et al. (2013) and Clegg et al. (2016).

The ChemCam telescope RMI is used to precisely image the LIBS targets. It produces a black-and-white image with the highest spatial resolution of any of the remote cameras on MSL; one RMI pixel corresponds to 19.6 μrad. These images are useful to visually identify mineral grains in the sample and provide textural context to the spectra acquired. The RMI is used both before and after acquiring a set of LIBS spectra, allowing interpretation of the textural nature of the area which produced the emission (Le Mouélic et al. 2015).

DATA ANALYSIS AND CALIBRATION OF CHEMCAM DATA

The individual spectra observed at each point are normally averaged together, discarding spectra from the first five laser shots at each point to avoid contamination from surface dust. The ChemCam spectra contain a large number of emission peaks representing atomic transitions of various elements present in the sample. Deconvolution of the spectra is best done using a multivariate approach. In general, LIBS data are subject to a variety of matrix effects, which can cause the intensity of the peaks to vary independently of elemental concentration (e.g., Clegg et al. 2009). Multivariate analysis is a useful tool to tackle these issues by using information from the entire spectrum. Initially during the MSL mission, a PLS2 algorithm was used to determine the major rock-forming elements. Following that, various PLS1 algorithms were used by the ChemCam team to increase the accuracy of the calibration. Most recently (including in this paper), ChemCam uses a combination of independent component analysis (ICA) (e.g., Forni et al. 2013), regression and submodel partial least squares (PLS; Clegg et al. 2009; Anderson et al. 2017) to derive quantitative compositions of targets on Mars. ICA components of LIBS spectra tend to isolate the emission lines of a single major element. ICA regression uses calibration curves for each element, derived by plotting the relevant ICA score against the composition of known laboratory targets in order to predict the composition of unknown targets. Submodel PLS is an extension of the PLS1 algorithm (Anderson et al. 2015). As chemical matrix effects vary with target composition, PLS models trained on a restricted composition range are often more accurate within that range than PLS models trained on a diverse suite of samples. Submodel PLS combines the results of multiple "submodels" optimized for restricted composition ranges to create a single model that has improved accuracy over the full range of compositions. The ICA and PLS submodel methods are trained using laboratory data collected from a suite of 408 well-characterized geostandards, and are combined using simple weighted means (Clegg et al. 2016).

The accuracy of ChemCam predictions is estimated based on the results obtained from a test set of laboratory samples, using the root-mean-square error (RMSE); see supporting information for further information. The test set for each major element was selected to have a distribution as similar as possible to the full training set used to generate the regression models (Clegg et al. 2016). The accuracy of ChemCam predictions varies with composition, as would be expected. Thus, rather than reporting a single RMSE per major element, a compositionally dependent RMSE is calculated, based on the test set samples similar in composition to the predicted composition of the unknown target. ChemCam's precision is significantly better than the estimated accuracy, and can be estimated based on repeated observations of the calibration targets on the rover. As we show in this paper, the comparison between APXS and ChemCam data on fine-grained sediments of basaltic composition gives added confidence in the accuracy of each technique.

Most applications of ChemCam elemental composition data use the reported values of each observation point. These are averages of the individual spectra from that point. In our application, we used compositions derived from single-shot spectra. We did this because compositions sometimes change within the 30 spectra obtained from each point due to the laser beam profiling from one mineral grain into another. Using single-shot compositions also provides a much larger database (e.g., >400,000 data points for the entire mission to date) on which to build contour plots and histograms.

To better view the distribution of the ChemCam data set, a scatter function algorithm was used to produce density contour plots. These are useful for examining the relative homogeneity of the data sets, as well as comparing and contrasting the focal point or focal points, as the case may be. Because the igneous rocks vary in grain size (Mangold et al. 2017) and the number of total number of spectra obtained per target vary, the LIBS data on individual rocks are often not sufficient to give an accurate whole rock composition (Dyar et al. 2011). For this reason, we combined the LIBS data based on the initial textural classifications rather than considering individual rocks. As mentioned above, the first few shots of each LIBS observation point are discarded because they are oftencontaminated by the Martian dust covering the sample.

See Table S1 in supporting information for more background information about precision and accuracy of ChemCam data.

ALPHA PARTICLE X-RAY SPECTROMETER

Another instrument on MSL that we make use of in this paper for major element analyses is the APXS on the rover arm turret. It utilizes ^{244}Cm sources to irradiate targets with a combination of alpha particles and X-rays (Gellert et al. 2009; Schmidt et al. 2014) measuring the resulting X-rays and the scattered alpha particles. This technique has a long heritage of planetary exploration with both the MER and the Sojourner rover of the Pathfinder mission including one of these instruments (Gellert et al. 2009). Unlike ChemCam, it analyzes a 1.6 cm diameter area, instead of microns. Major elements—Si, Ti, Al, Fe, Mg, Mn, Ca, K, Na, P, S, and Cl— are normalized to 100 wt%. Light elements are not included, but as the samples in question are relatively anhydrous, we are able to directly compare the data sets. The APXS errors we list here measure precision; accuracy is shown in the supporting information. The feldspar-rich extrusive samples we discuss in this paper have not been analyzed by APXS but its data are important as a comparison at the low SiO_2 end of the Gale data in particular.

RESULTS

Figure 2 shows a HiRISE (High Resolution Imaging Science Experiment) mosaic of the Curiosity path en route to Mount Sharp (Aeolis Mons), with some key locations of igneous float rocks and sedimentary targets marked. During the first 1000 sols, a large amount of data—over 700 ChemCam targets containing both LIBS spectra and RMI images—were collected. Twenty-five igneous float rocks were identified in MastCam and RMI images (Fig. 3) up to sol 553. A textural classification was described in Sautter et al. (2014). One type of igneous rock is volcanic and includes dark, mainly aphanitic basaltic samples (e.g., Ashuanipi float rock, Fig. 3). Some possible vesicles are evident, e.g., as in the Tully target. Coarse-grained (>500 μm median grain size; Sautter et al. 2015), feldspar-rich samples are also notably present, such as the Robin Hood and the Harrison conglomerate clasts (sols 365 and 514). Feldspar was identified on the basis of the compositions as well as the pale color and tabular crystal forms (Williams et al. 2013; Sautter et al. 2015). Subsequent LIBS compositional analyses have supported this identification (Gasda et al. 2016; Cousin et al. 2017).

Frequency histograms of major element compositions and Fig. 4 illustrate the differences in composition between the igneous float rock and the combined sedimentary outcrop samples. Individual

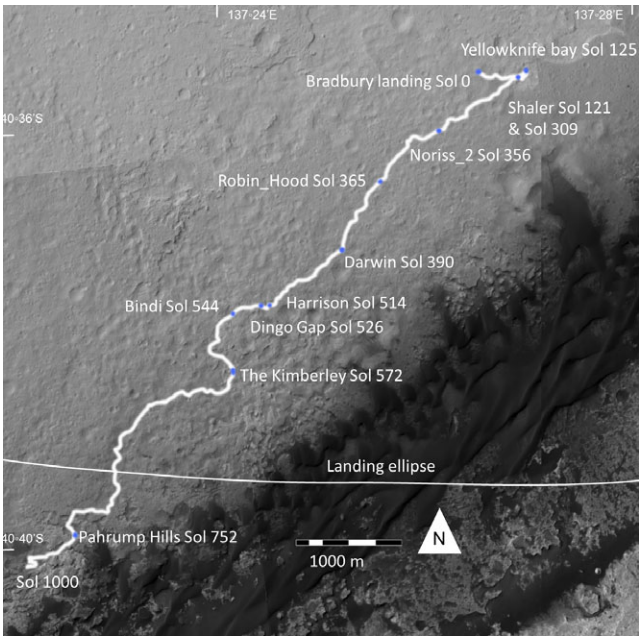

Fig. 2. HiRISE view showing MSL Curiosity rover's progress since landing with various points of interest marked—sedimentary outcrops and representative igneous locations. HiRISE images ESP_027834_1755_RED, ESP_035917_1755_RED, and ESP_028401_1755_RED were used to produce this map.

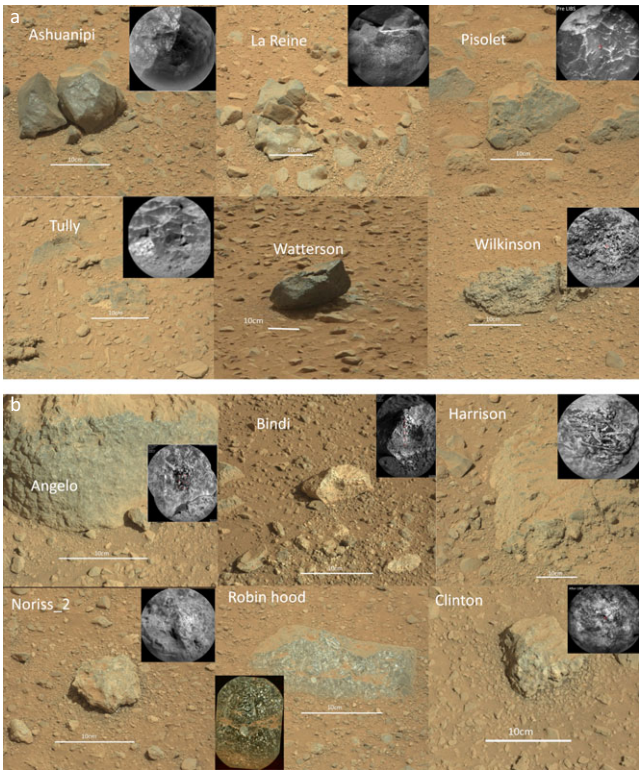

Fig. 3. Samples from the two endmember groups of igneous rocks. (a) Ashuanipi (sol 337), La Reine (sol 346), Pisolet (sol 332), Tully (sol 456), Watterson (sol 329), and Wilkinson (sol 365) are basaltic, while (b) Angelo (sol 553), Bindi (sol 544), Harrison (sol 514), Noriss_2 (sol 356), Robin Hood (sol 365), and Clinton (sol 512) are trachybasaltic. These images were taken from MastCam and the ChemCam RMI images.

coarse-grained igneous rocks do not have enough observation points to give a whole rock composition to high accuracy, e.g., Dyar et al. (2011). The histograms are produced from analyses corresponding to each individual laser pulse, which represent compositions at the 350–550 μm scale. In Fig. 4 (and Tables 1 and 2) igneous plots, the mean compositions of the texturally defined basalt (n = 6 samples and 538 spectra) and trachybasalt (n = 7 samples and 1011 spectra) are labeled. The total number of igneous sample spectra in Figs. 4 and 5 is 5787, thus including some samples (13) where the textural distinction between basalt and trachybasalt was not considered to be clear enough to be used in the mean endmember calculations.

Density contour plots (Fig. 5)—where each contour represents an equal amount of data—reveal the main foci of data. Within the Gale igneous samples, the two endmembers (i.e., broadly, fine-grained basaltic and more coarse-grained, feldspar-rich; Sautter et al. 2014) differ compositionally in line with what would be expected from the observed mineralogy. The feldspar-rich group has relatively high SiO_2, Al_2O_3, and alkalis (particularly Na_2O), and is low in FeO and MgO. The igneous samples trend from the basaltic compositions focused at around 47–51 wt% SiO_2, to a local maxima (Figs. 5 and 6) of ~55 wt% (53 ± 5 wt%) SiO_2 in the more abundant feldspar-rich group (Table 1). The trachybasalt and basaltic textural groups were used as a starting point to calculate the two equivalent compositional endmember means for the igneous samples, and a bulk average of the sedimentary targets was also calculated. The Gale trachybasalt composition is analogous to some terrestrial trachybasalts (Figs. 5 and 6) though terrestrial trachybasalt analogs are relatively richer in MgO compared to FeO, as expected for an Earth–Mars igneous comparison (e.g., McSween 2002). Figure 6 is a total alkali versus silica (TAS) plot with comparison fields for terrestrial rocks—oceanic island basalts (OIB), mid-ocean ridge basalts, and also trachybasalts from a variety of continental and oceanic terrains (Baker 1969; Humphreys and Niu 2009; Gale et al. 2013) are also plotted. The OIB field lies at a $Na_2O + K_2O$ combined content similar to the Gale basalts.

The two igneous maxima may each include additional igneous subcomponents, as proposed by Sautter et al. (2015) and Cousin et al. (2017). In

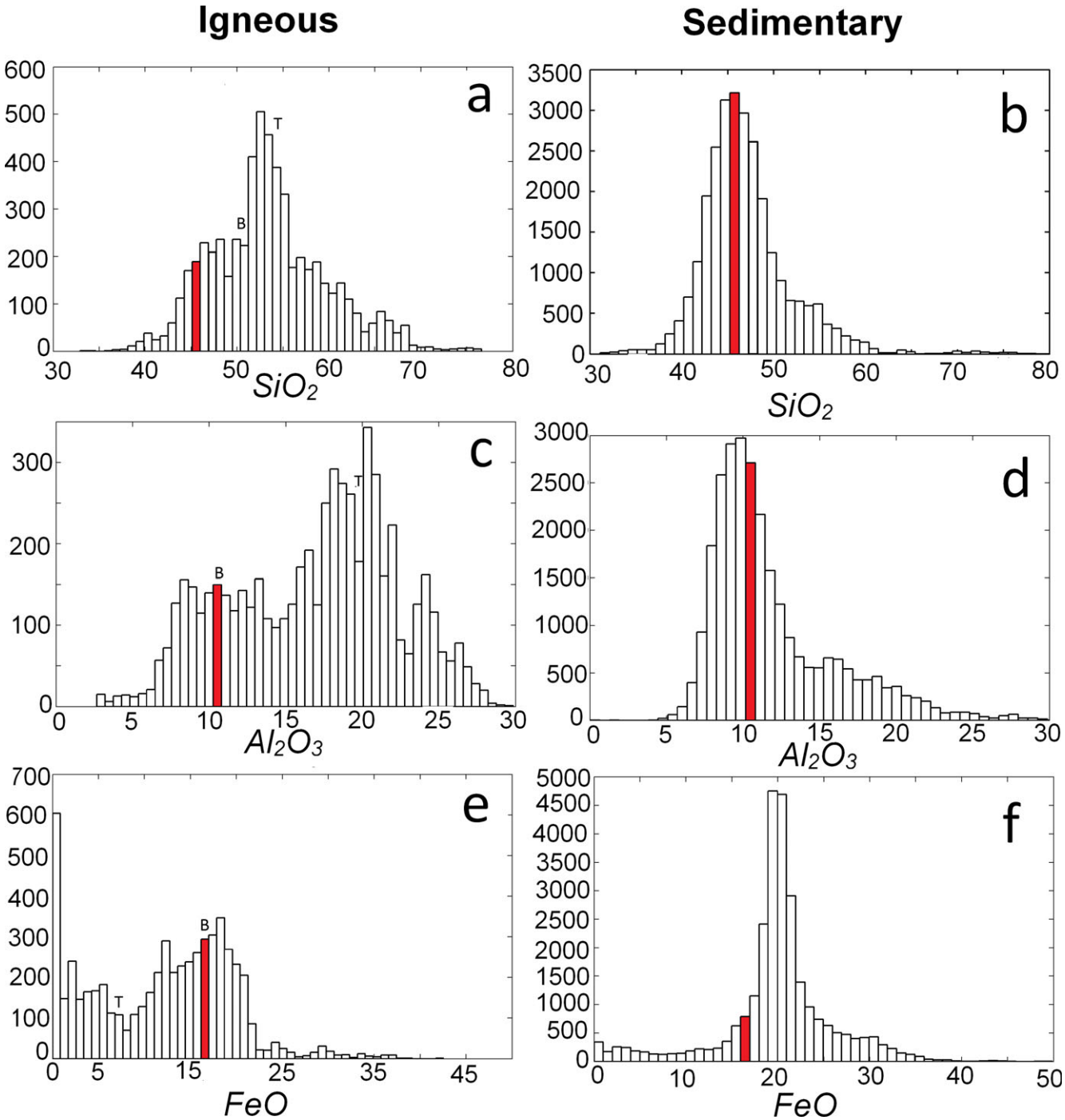

Fig. 4. Histograms showing the distribution of sedimentary and igneous observations for each major-element oxide. Only single-shot spectra giving major-element totals between 95 and 105 wt% were included; the red column is the mean MER Spirit APXS data from targets encountered at Gusev Crater (MER PDS). For igneous plots a, c, e, g, i, m, the total number of spectra = 5787 and for sedimentary plots b, d, f, h, j, l, n, the number of spectra = 27,448. There are 1011 spectra from texturally identified trachybasalt samples and 538 from basalt, the remainder of spectra in the igneous plots are from samples where the textural distinction between trachybasalt and basalt was unclear. Error E = RMSE for CCAM data and is a measure of accuracy and P = CCAM precision; see supporting information for more information. T and B are the trachybasalt and basalt mean compositions (Tables 1 and 2) with groups based on the textural classification.

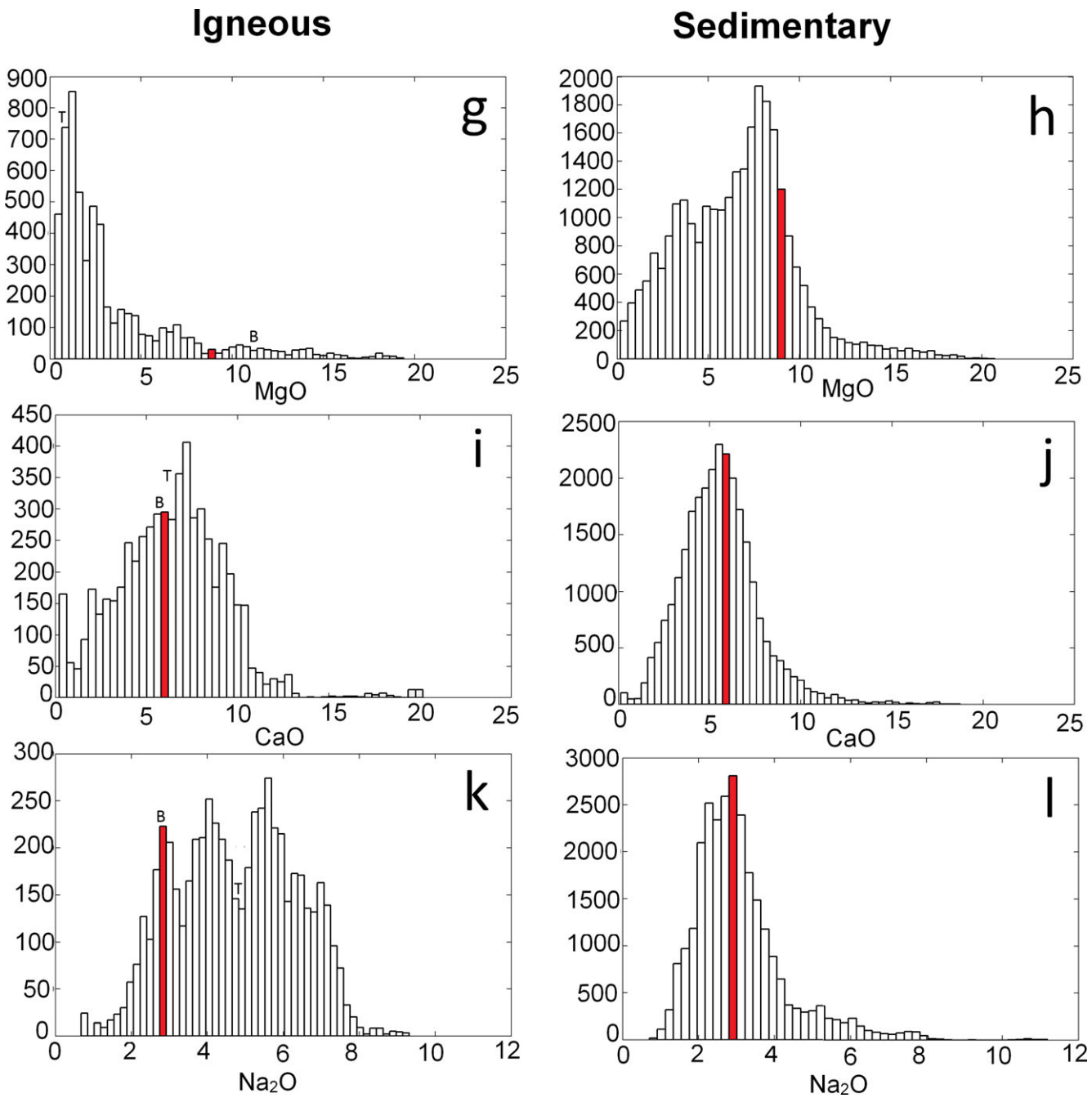

Fig. 4. Continued.

particular, the unique Bindi sample (Fig. 3) contains ~80% feldspar and may be a cumulate (e.g., Cousin et al. 2017). However, because the LIBS data on individual rocks are often not sufficient to give an accurate whole rock composition (Dyar et al. 2011) and imaging data are also sometimes limited, we used the statistical, grouping approach based on the density contours and frequency histograms. We discuss the samples below as simple compositional endmembers, and we will study the potential relationship between them and other Martian basaltic rocks.

The shergottites generally have considerably lower Al_2O_3 contents than these Gale igneous samples which have maxima at 11 and 22 wt%. The different shergottites—although comprised of a diverse range of samples and modal mineralogies—have a smaller range of SiO_2 than the Gale igneous samples (Figs. 4, 5, and 6). The shergottites also have low combined

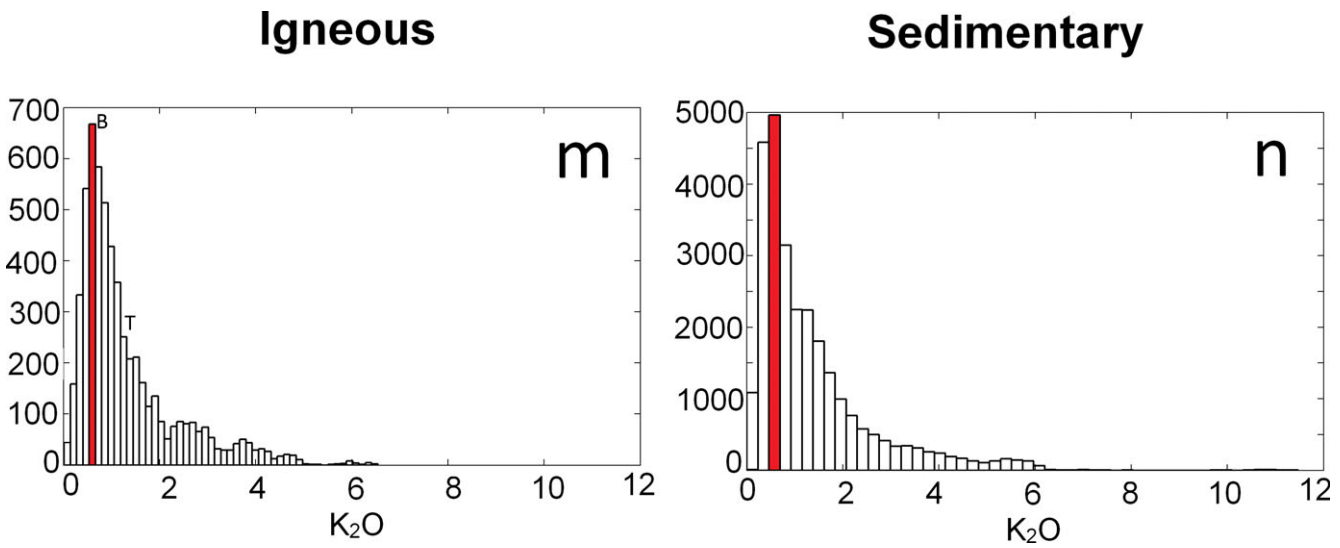

Fig. 4. Continued.

$Na_2O + K_2O$ contents compared to the Gale igneous rocks we are studying which have $Na_2O + K_2O$ of 4–6 wt% (Fig. 6). The trachybasalt samples also have a notably low MgO (average 1.6 wt%, Table 1) and a lower focus of Mg# at ~27 than the MER Spirit (Mg# = 52), (Figs. 4 and 5; Table 2), but the Gale basalt endmember focus of Mg# at ~54 is similar to the MER compositions. We note these foci of Mg# do not preclude a wider spread from individual targets. As we argue in the next section, the crystal-melt fractionation the trachybasalt parent rocks underwent from basaltic melt precursors gave them the lower average MgO and Mg# composition foci.

The sedimentary strata have been analyzed to provide outcrop data along the Gale traverse, which we use to compare with our igneous samples' compositions. The individual stratigraphic units are described in Grotzinger (2013), Rice (2014), Anderson et al. (2015), Le Deit et al. (2016), and Mangold et al. (2016). These sediments are fluvio-lacustrine mudstones and coarser sediments, which have sampled source areas around Gale Crater (Grotzinger et al. 2015). The sedimentary outcrop analyses have a clear LIBS focal point of SiO_2 at 45 wt%, similar to the basaltic endmember of the igneous samples. Likewise for Al_2O_3, the sedimentary set has a well-defined compositional density peak at 10 wt%, but as noted above, the igneous data have a less well-defined peak and ranges 6–25 wt% Al_2O_3. For FeO, the sedimentary data (peak at 19 wt%) have a wider distribution than the igneous rocks, but match those of the shergottite meteorites. The CaO distributions are broadly similar with the sedimentary outcrops having a slightly lower mean (5.5 wt%) than the igneous float samples' mean (6.4 wt%). The Gale basaltic igneous and sedimentary samples both give further evidence for the importance of an Fe-rich, Al-poor, moderately alkali-rich basaltic composition in the Martian highlands, distinct from the more alkali-poor shergottites. APXS data from numerous sedimentary targets are in agreement with the focal point at 45 wt% SiO_2. The additional trend toward extreme CaO enrichment in the sediments reflects the presence of abundant Ca sulfate veins of diagenetic origin (Nachon et al. 2014; Schwenzer et al. 2016) and is not directly related to the bulk silicate and oxide compositions of the sediments.

CRYSTAL FRACTIONATION MODEL

In order to test crystal fractionation controls on the igneous trends identified in Figs. 5 and 6, a simple model (described below) was used to simulate the igneous compositional trends through crystal fractionation. The model subtracted olivine and pyroxene from the Spirit MER composition of the Humphrey sample, a representative Adirondack class, olivine-rich Martian basalt. This composition (Gellert et al. 2009) was normalized to 100%, and then 10% augite was subtracted. The result was then renormalized and a series of olivine subtractions took place every 10% between 0 and 40%. An olivine composition of SiO_2 = 32 wt%, FeO = 44 wt%, and MgO = 24 wt% was used to reflect the Fe-rich, low-Mg nature of the environment. The Mg# of the olivine (50) used in the crystal fractionation model is within the range suggested by Mossbauer spectroscopy (Morris et al. 2006; Filiberto et al. 2008) for the Adirondack basalts on the MER Spirit landing (60 ± 10). For the augite

Table 1. Mean bulk and normative compositions of basalt and trachybasalt endmembers (ChemCam Data from MSL PDS).

	Basalt	Trachybasalt	Sedimentary
Mean			
SiO_2	51.4	55.2	49.6
TiO_2	1.2	0.8	1
Al_2O_3	10.7	19.8	14.3
FeO	17.7	7.7	18.7
MgO	11.8	1.6	5.8
CaO	5.6	6.4	5.3
Na_2O	3	5.4	3.3
K_2O	0.6	1.2	1.3
Total	101.9	98	99.2
Mg#	54.3	27	35.6
One standard deviation			
SiO_2	2.6	3.5	4.4
TiO_2	0.9	0.2	0.3
Al_2O_3	4	2.5	3.6
FeO	2.4	5.6	5.4
MgO	4.1	1	2.9
CaO	1.4	2.4	2.2
Na_2O	0.9	1.3	1.1
K_2O	0.5	0.9	1.1
Total	2.8	1.9	2.6
Fe^{3+}/(total iron)	0.1	0.2	0.1
Plagioclase	39.3	39.3	71.9
Orthoclase	3.7	3.7	6.9
Diopside	11.1	11	4.5
Hypersthene	24.7	28.4	11
Olivine	18.3	11.9	1
Ilmenite	2.3	2.3	1.5
Magnetite	2.9	5.7	1.3
Total	102.1	102.3	98.1

Basalt and trachybasalt fields are the average of each texturally defined class's composition. Sedimentary is a mean of all sedimentary data from the first 1000 sols (MSL PDS).

subtraction, a composition of SiO_2 = 42 wt%, FeO = 19 wt%, MgO = 14 wt%, and CaO = 24 wt% was used due to a similar Mg# to Humphrey. This model matches well with the apparent trend (Figs. 5 and 6) of igneous compositions, for major elements and Mg# of 54-27, from the lower silica igneous peak near the Gusev-like basaltic composition to the trachybasalt peak, suggesting a fractionation trend based on the removal of olivine. The key link between the fractionation of olivine and the Gale compositional trend raises the issue of the identification of olivine in Gale rocks. Although CheMin has identified variable amounts of olivine in some Gale sediments (Vaniman et al. 2014), ChemCam has not identified discrete olivine phenocrysts in the igneous samples or detrital grains in the sedimentary rocks. The absence of olivine in the igneous samples is to be expected for silica-saturated, low-MgO trachybasaltic bulk compositions. Within the basaltic igneous rock, and sediments, the absence of pure olivine compositions—or identified olivine phenocrysts in images—may be due to the grain size of the olivine being less than the laser beam width of 350–500 μm. It may also be the case that there has not yet been a suitable MAHLI, RMI image on a fresh face on the limited number of basaltic igneous samples.

CIPW NORMATIVE COMPOSITIONS

Table 1 presents CIPW weight normative values calculated from the textural endmember mean compositions, together with a realistic set of $Fe^{3+}/(Fe^{3+} + Fe^{2+})$ contents, i.e., 0.1–0.2 (e.g., Schmidt et al. 2013, 2014). Figure 7 shows these results plotted on a Yoder and Tilley (1962) basalt tetrahedron. The tetrahedron spans the parameter space between normative diopside, nepheline, quartz, albite, enstatite, and forsterite. This divides the tetrahedron volume into three sub tetrahedra. Both of the Gale representative igneous compositions fall between the plane of silica saturation (Di, Ab, and En) and the plane of silica undersaturation (Di, Ab, and Fo) indicating that a significant fraction of the igneous Gale rocks is olivine and hypersthene normative, having affinities with terrestrial silica-saturated, olivine tholeiites. CIPW norms are generally used to estimate the mineralogical composition of anhydrous igneous rocks, such as these. We do not consider normative mineralogies of the averages of Martian sedimentary rocks because of the presence of hydrous mineralogy. However, as there is strong evidence (McLennan 2003; Bridges et al. 2015) for dominantly isochemical alteration in the sedimentary rocks from the early part of the mission, we do compare the sediments on the TAS plots with igneous fields as a useful way of contrasting the igneous float rock compositions.

DISCUSSION

Mars has generally been considered to have a dominantly basaltic composition crust on the basis of over 40 yr of Martian meteorite analyses, orbiting spectral observations, and previous landed missions (e.g., Adams 1968; McSween et al. 1999; Bandfield 2000; Bibring and Erard 2001; Bridges and Warren 2006; Karunatillake et al. 2006). However, Dreibus and Wänke (1985) suggested that the Martian interior is alkali-enriched compared with the Earth, and some alkali-rich rocks have been found on Mars with McSween and Ruff (2006) demonstrating that moderately alkaline-rich basalt, trachybasalt, was present at the MER Spirit landing site. In addition, Adirondack class, subalkaline, olivine-rich basalts, like

Table 2. Comparison of the compositions of the mean endmembers of the igneous samples with MER.

Data set	SiO_2	TiO_2	Al_2O_3	FeO	MgO	CaO	Na_2O	K_2O	P_2O_5	SO_3	Cl	MnO	Cr_2O_3	Total	Mg#
Mean spirit APXS[a]	45	1	10.5	15.5	9.3	6.2	3	0.4	1.4	6.1	0.9	0.3	0.3	99.9	51.7
MER—Wishstone[a]	43.8	2.6	15	11.6	4.5	8.9	5	0.6	5.2	2.2	0.4	0.2	0	99.9	40.9
MER—Bounce[a]	47.5	0.7	10.7	14.2	7.6	9.8	2.2	0.3	0.9	4.6	0.9	0.4	0.1	100	48.8
MER—Humphrey[a]	46.3	0.6	10.8	18.6	9.5	8.2	2.8	0.1	0.6	1.1	0.3	0.4	0.7	100	47.6
MSL—APXS[b]	45.5	0.9	9.6	17.8	7.4	5.9	2.9	1.1	1	5.8	1.1	0.4	0.4	99.7	42.6
Basaltic endmember[b]	51.4	1.2	10.7	17.7	11.8	5.6	3	0.6	N/A	N/A	N/A	N/A	N/A	N/A	54.3
Trachybasaltic endmember[b]	55.2	0.8	19.8	7.7	1.6	6.4	5.4	1.2	N/A	N/A	N/A	N/A	N/A	N/A	27.0

Targets texturally identified as basaltic and trachybasaltic use the mean of the ChemCam spectra for the relevant targets. ChemCam PLS/ICA does not return values for P, S, Cl, Mn, or Cr.
[a]MER PDS.
[b]MSL ChemCam LIBS Planetary Data System.

"Humphrey" used in our model, show a complex record of planetary differentiation. Furthermore, relatively alkali-rich basalts were predicted to be on the surface of Mars based on the mineralogy and mineral chemistry of the chassignites (Nekvasil et al. 2007), and a connection between basalts at Gusev Crater and the chassignites was suggested based on mineral chemistry and results of experimental crystallization studies (Filiberto et al. 2008; Nekvasil et al. 2009). Although the majority of the 90 known Martian meteorites are subalkaline, the impact regolith breccia NWA 7034, NWA 8114, and pairs have a high abundance of K-feldspar and contain alkali basalt clasts (Humayun et al. 2013; Santos et al. 2015), suggesting that the parental magmatic crust to some of the clasts in the rock was alkali-rich. The Yoder and Tilley basaltic tetrahedron in Fig. 7 uses CIPW weight-normative compositions to show the relationships between igneous data (Yoder and Tilley 1962). The critical plane Di–Fo–Ab has fundamental petrological significance in that it is an equilibrium thermal divide across which silicate liquids cannot pass at the relatively low pressures associated with shallow crustal settings. Thus, the silica-saturated rocks associated with the Gale trachybasalts cannot be co-genetic with any silica-undersaturated, alkaline igneous rocks in the Gale catchment. Magmas undergoing tholeiitic fractionation become saturated with Fe as their silica contents increase during fractional crystallization and begin crystallizing iron oxides (Nicholls and Ringwood 1972). The residual magma becomes progressively enriched in alkali metals as the melts evolve toward silica and alkaline-rich compositions. The tholeiite fractionation trend can produce a wide range of igneous rock types including trachybasalts, trachyte, and rhyolite, such as shown by the Shishaldin volcanics in the Aleutian Islands, Aleutians (Cox et al. 1970; Spulber and Rutherford 1983; Whitaker et al. 2005; Zimmer et al. 2010). The olivine-dominated fractional crystallization trends shown for the major elements in Fig. 5 are consistent with such differentiation taking place. Recent discoveries of the high-temperature silica polymorph tridymite by Curiosity (Morris et al. 2016)—although not diagnostic of a particular melt composition—are consistent with the presence of more fractionated tholeiitic igneous rocks—as yet unidentified in whole rock samples—in the Gale catchment.

Sedimentary units in the early part of the MSL mission—Sheepbed, Shaler, Darwin, and Pahrump Hills, sols 126–923 (Grotzinger et al. 2015)—have compositions similar to those of the MER APXS olivine-rich basalts' data from Gusev Crater. The Gale sedimentary units do, however, show notable compositional differences between and within each other. For instance, Mangold et al. (2016) used ChemCam data to show that conglomerates in Darwin had source regions with varying Na/K ratios. Alkali enrichment was seen within the Shaler Facies 7 and Kimberley units, which were relatively K-rich and also in the latter case known to be sanidine-bearing from CheMin XRD (Anderson et al. 2015; Thompson et al. 2016; Treiman et al. 2016). Similarly, APXS analyses of the Jake_M float sample (sols 46–47) suggest it is sufficiently enriched in sodium that it is either a silica-undersaturated, nepheline-normative, alkaline igneous rock (as originally suggested by Stolper et al. 2013), or a sedimentary float rock which has sampled alkaline igneous minerals from the catchment area. The origin of those alkali enrichments is beyond the scope of our paper on silica-saturated igneous rocks, and as shown by the basalt tetrahedron plot (Fig. 7), there is no clear link between them. However, we note that silica-undersaturated, alkaline-rich rocks are likely to be part of the Peace Vallis catchment area (Treiman et al. 2016) while not being the dominant Gale igneous signature. Juxtaposition of distinct alkaline and tholeiitic lavas is

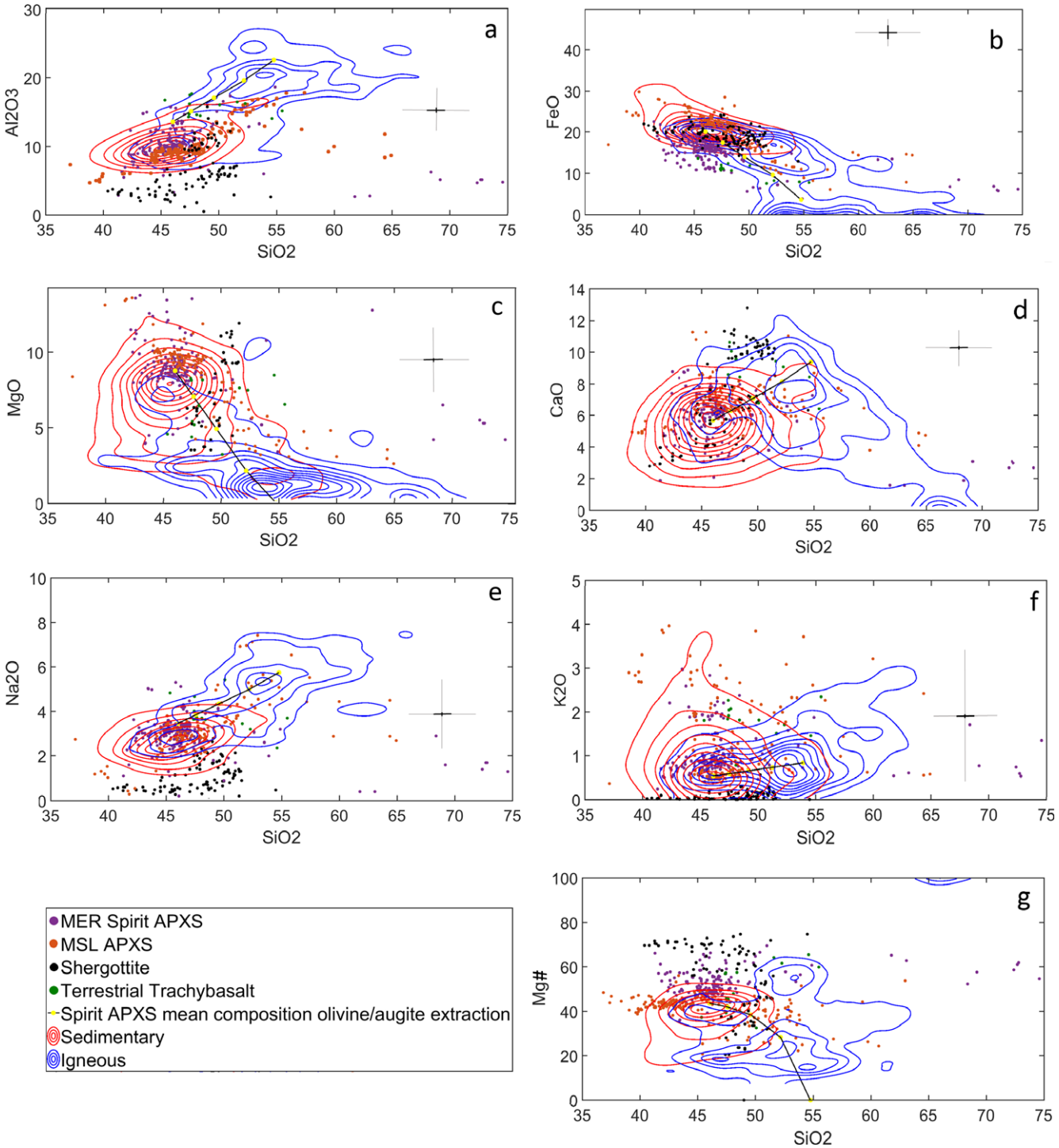

Fig. 5. Contour plots a–g showing the distribution of major-element oxides for the sedimentary and igneous compositional groupings. Each contour level contains an equal fraction of data. Individual spectra data were used with the major-element oxide totals between 95 and 105%. The first five spectra on each observation point were ignored as they contain a high percentage of Martian dust giving an unrepresentative view of the target composition. The olivine subtraction model is marked with each point on the black line marking 10% olivine extractions moving from left to right. Terrestrial trachybasalts are included from the literature (Baker 1969). Light crosses on each plot show the RMSE error (accuracy) for each ChemCam oxide and darker crosses show precision; see supporting information for further information. MER data from Spirit at Gusev.

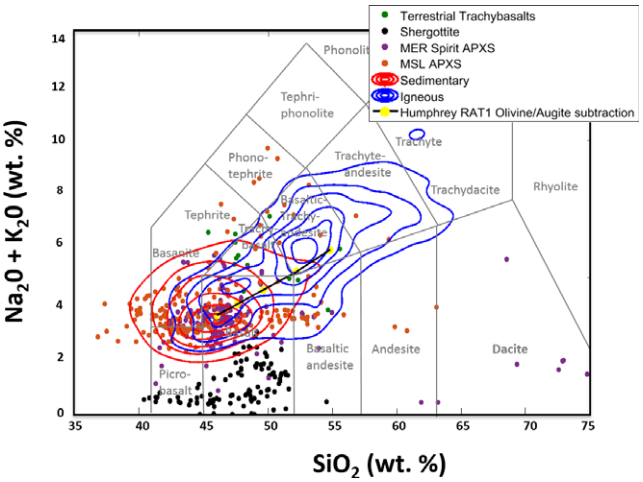

Fig. 6. TAS plot comparing the sedimentary and igneous groupings with MSL ChemCam and MER APXS data, along with Martian shergottite meteorite data. Also shown are terrestrial trachybasalts from the literature. Each contour level contains an equal fraction of data. Single-shot data with major-element totals of 95–105% were used. Model shown subtracting olivine and pyroxene from the mean of a representative Spirit MER APXS target Humphrey RAT1 (MER PDS). This mean was normalized to 100% for the model and then 10% augite composition was subtracted. This was again renormalized and then a series of 10% olivine subtractions between 0 and 40% shows a trend matching the igneous compositions. Terrestrial mid-ocean ridge basalts (Gale et al. 2013) and ocean island basaltic compositions (Humphreys and Niu 2009) are also plotted. The cross shows CCAM RMSE (accuracy), and APXS errors (percentage error of total) are detailed in the supporting information.

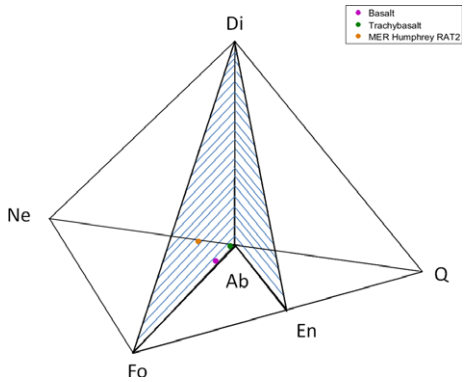

Fig. 7. Yoder and Tilley basalt tetrahedron (Yoder and Tilley 1962) showing that Gale igneous rocks fall between the olivine and silica normative planes, and so have silica-saturated compositions. Mean compositions of the spectra in the subcategorized basaltic and trachybasaltic groups were used for the CIPW norm (Table 1). Di = diopside; Ne = nepheline; Q = quartz; Ab = albite; En = enstatite; Fo = forsterite. Humphrey composition from MER PDS and McSween and Ruff (2006).

known on Earth, and is characteristic of ocean island settings (Delong and Hoffman 1975; Floyd et al. 1991). An important overall observation from Gale is that coarse-grained sediments (e.g., conglomerates and coarse-grained sandstones) are more felsic (enriched in silica and alkalis), while fine-grained material, such as the Yellowknife Bay Mudstone (McLennan et al. 2014; Mangold et al. 2015), is more mafic (Mangold et al. 2016), much closer to the canonical average Mars composition (Taylor and McLennan 2009). This may suggest that regions closer to Gale, which would be the source of larger clasts and coarser grained material, have more felsic compositions, while catchment regions farther from Gale, represented by more abraded, finer grained material, are more mafic.

The similarity between MSL sedimentary detrital material and MER Spirit basalt data indicates that their parental melts had mantle source regions of similar composition and nature, but distinct from those associated with the more alkali- and Al-poor shergottites. The latter are often considered to have been derived from depleted mantle melts underlying the northern lowlands and Tharsis, and the majority crystallizing <600 Myr ago (e.g., Nyquist et al. 2001; McSween et al. 2003). In contrast, McSween and Ruff (2006) described mantle partial melting controls leading to primitive picritic basalts (like the Humphrey sample) in Gusev. The Gale igneous samples that are the topic of our paper are related to this type, rather than shergottites, through crystal-melt fractionation.

WATER AND HYDRATED MINERALS IN MARTIAN MAGMAS

The water content of magmas is a critical control factor on their petrogenesis. For instance, Whitaker et al. (2005) reported their experimental evidence that tholeiitic basalt can give rise to alkaline magma if crystallized >4.3 kbar and with magmatic water contents above 0.4 wt%. However, until recently, there has been little consensus about the water content of Martian basaltic magmas. The shergottites typically contain less water (<350 ppm H_2O; e.g., Leshin and Epstein 1996) than their terrestrial basaltic counterparts (2000–20,000 ppm H_2O; e.g., Saal et al. 2002). The magmatic water contents of glassy olivine-hosted melt inclusions in primitive basaltic shergottites are similarly low, at <250 ppm H_2O (Usui et al. 2012, 2015; Collinet et al. 2015). However, to some extent, magmas will have degassed upon eruption (McSween et al. 2001; Beck et al. 2004; Herd et al. 2005; Udry and Howarth 2016). Because of this inherent uncertainty, estimates of water in Martian magmas range from nearly anhydrous to 2 wt% dissolved H_2O (e.g., see review Filiberto et al. 2016a, 2016b). Recent investigations of hydrous and halogen-bearing minerals (in particular apatite) have helped to constrain the water

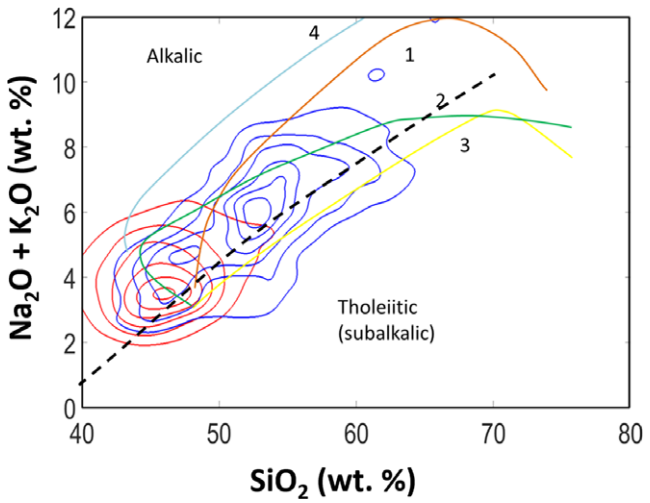

Fig. 8. Total alkalis versus silica diagram showing four major trends from Whitaker et al. (2005) and Nekvasil et al. (2007). (a) Silica-saturated Na-rich, (b) silica-saturated K-rich, (c) ocean island tholeiitic, and (d) silica-undersaturated Na-rich trends (Nekvasil et al. 2007). The contours are single-shot ChemCam compositions of igneous samples (blue) and sedimentary (red) samples—see Figs. 5 and 6. Trend 2 (5 kbar, dry conditions) corresponds most closely to the igneous trend in the Gale samples studied in this paper, though with slightly lower alkalis. Dotted line represents the alkali/subalkali saturation divide from Irvine and Baragar (1971).

contents of pre-eruptive Martian magmas, and the results are consistent with a drier interior (Gross et al. 2013; Filiberto et al. 2016a; McCubbin et al. 2016). Recently, Filiberto et al. (2016b) calculated a basalt source region that is 56 ± 60 ppm H_2O.

Such a low water content is consistent with the notably anhydrous mineralogy of the igneous components of the Gale sedimentary assemblages. None of the drillhole CheMin XRD analyses of sedimentary outcrop targets have revealed any amphibole or mica (e.g., Vaniman et al. 2014; Treiman et al. 2016; Rampe et al. 2017). Micas have been inferred from ChemCam observations indicating co-enrichments of Al and F (Forni et al. 2015; Le Deit et al. 2016); however, in these sheet silicates, F can substitute for OH. Amphibole may also have been observed by ChemCam, but conclusions are not definitive due to the qualitative nature of the hydrogen observations (Schroeder et al. 2015) and the fact that amphibole major-element compositions potentially overlap with other common minerals or combinations of minerals.

In contrast, one argument that has been put forward for volatile-rich Gale magmas is from modeling of the source material for the Jake_M float rock, e.g., Collinet et al. (2015). Based on the (questionable) assumption that this rock is igneous, a water content of at least 0.5–1 wt% H_2O could be required to achieve the relatively high Al/Mg ratio observed in this rock (Stolper et al. 2013). However, in line with the current understanding of low water contents in Martian magmas, the uncertain origin of the Jake_M sample, and the absence of any obvious evidence from ChemCam data for amphibole or mica in the igneous float rocks, we suggest the parental Martian melt to the trachybasalts was anhydrous.

TERRESTRIAL AND EXPERIMENTAL ANALOGS

If Mars has always lacked plate tectonics as is generally accepted (Banerdt et al. 1982; Karlsson et al. 1992; Mezger et al. 2012), then intraplate magmatism will be most relevant for interpreting our results. In the terrestrial environment, intraplate magmas are often part of diverse groups of magmas including from basalt to rhyolite, alkaline and tholeiitic compositions (e.g., Whitaker et al. 2005). Results from data from Gusev Crater and the Spirit Mars Exploration Rover have shown samples with some similarities to these terrestrial basalts such as OIB. Oceanic island magmatic provinces are associated with both tholeiitic and alkaline magmas (Wilson 2007) and so are useful analogs for Gale igneous rocks. However, we note that this analogy has limitations because terrestrial primitive OIB has H_2O contents of 2000–8000 ppm (Johnson et al. 1994; Dixon and Clague 2001), far higher than the likely anhydrous magmas under consideration here. Terrestrial trachybasalts are found in a range of alkaline and tholeiitic environments. Previous experimental work has investigated the fractionation conditions likely to be experienced in the Martian igneous environment. Nekvasil (2004), Nekvasil et al. (2007), and Whitaker et al. (2005) tested melt fractionation, starting from hawaiite compositions associated with ocean islands and continental hotspots. Those authors demonstrated that there are four major trends that these compositions can follow. They are (1) silica-saturated, Na-rich; (2) silica-saturated, K-rich; (3) ocean island tholeiitic; and (4) silica-undersaturated, Na-rich. Comparing these trends to our ChemCam data helps constrain the nature of the melt source and fractionation conditions. The ChemCam data parallel quite closely the Curve 2 trend in Whitaker et al. (2005, 2007) in Fig. 8, which is representative of silica-saturated, K-rich basalt. Fractionation of a tholeiitic parent liquid at 4.3 kbar (i.e., a mid-crustal pressure on Mars, Nimmo and Stevenson 2001) with moderate water contents (~0.3 wt%) replicates the silica-enrichment segment of Trend 2. This part of the trend continues from ferrobasalt to potassic rhyolite (Whitaker et al. 2005, 2007), again raising the possibility of more fractionated igneous samples in Gale that have yet to be identified.

This suggests that the Gale basalt to trachybasalt igneous assemblage is associated with fractionation at low crustal pressures from low H_2O, silica-saturated tholeiitic magmas. Similarly, Nekvasil (2004) showed that under shallow crustal conditions, the abundance of early olivine produces strong silica enrichment and subalkalic total alkalis to silica ratios in evolved basaltic rocks. The dotted line on Fig. 8 represents the alkali saturation divide from Irvine and Baragar (1971). That line suggests that the Gale igneous rocks are close to the boundary of tholeiitic and alkaline lavas but as argued previously, this 2-D plot has limitations in firmly distinguishing alkaline from tholeiitic melts (Delong and Hoffman 1975). The crystallization sequence of an Fe-rich tholeiitic basalt magma at low pressure starts by being dominated by olivine extraction (Grove and Baker 1984). Following the olivine extraction plagioclase dominates. Thus, our model of initial olivine-dominated fractionation (to create feldspar-rich trachybasalts) is realistic.

CONCLUSIONS

1. The ChemCam and textural observations of igneous float rocks and conglomerate clasts in the first 530 sols of the Curiosity rover traverse in Gale Crater have led to identification of extrusive basalts and trachybasalts.
2. ChemCam data show that the samples identified texturally as basaltic have an average SiO_2 content of about 47–51 wt%, Mg# = 54, and those identified texturally as trachybasalts, $\sim$55 wt% (53 ± 5 wt%), Mg# focus at 27. This range in composition is consistent with olivine-dominated crystal fractionation from a subalkaline, Fe-rich basaltic melt similar to the composition of Adirondack class basalts seen at Gusev Crater.
3. The Gale melts associated with the basalt–trachybasalts were silica-saturated and tholeiitic. Our model shows that these are consistent with a formation under Mars crustal pressure (e.g., 4.5 kbar) and low H_2O conditions. These affinities, together with the likely existence of alkaline, silica-undersaturated igneous rocks in other parts of the Gale catchment, are consistent with a terrestrial intraplate analogy for Gale magmatism.

Acknowledgments—The MSL engineering, ChemCam, and science teams are thanked for enabling the successful acquisition of the data reported in this paper. PHE, SPS, and JCB acknowledge funding from UKSA. Funding in the United States was supported by NASA through the Mars Exploration Program. This paper benefited from two anonymous reviews.

Editorial Handling—Dr. Gordon Osinski

REFERENCES

Achilles C. N., Vaniman D. T., Blake D. F., Bristow T. F., Rampe E. B., Ming D. W., Chipera S. J., Morris R. V., Morrison S. M., Downs R. T., and Fendrich K. V. 2016. Mineralogy of eolian sands at Gale Crater (abstract #2532). 47th Lunar and Planetary Science Conference. CD-ROM.

Adams J. B. 1968. Lunar and Martian surfaces: Petrologic significance of absorption bands in the near-infrared. *Science* 159:1453–1455.

Anderson R. C., Bridges J. C., Williams A., Edgar L., Ollila A., Williams J., Nachon M., Mangold N., Fisk M. R., Schieber J., Gupta S., Dromart G., Wiens R. C., Le Mouélic S., Forni O., Lanza N. L., Mezzacappa A., Sautter V., Blaney D. L., Clark B., Clegg S., Gasnault O., Lasue J., Léveillé R., Lewin E., Lewis K.W., Maurice S., Newsom H., Schwenzer S. P., and Vaniman D. 2015. ChemCam results from the Shaler outcrop in Gale crater, Mars. *Icarus* 249:2–21.

Anderson R. B., Clegg S. M., Frydenvang J., Wiens R. C., McLennan S., Morris R. V., Ehlmann B., and Dyar M. D. 2017. Improved accuracy in quantitative laser-induced breakdown spectroscopy using sub-models. *Spectrochimica Acta Part B: Atomic Spectroscopy* 129:49–57. https://doi.org/10.1016/j.sab.2016.12.002.

Baker I. 1969. Petrology of the volcanic rocks of Saint Helena Island, South Atlantic. *Geological Society of America Bulletin* 80:1283.

Bandfield J. L. 2000. A global view of Martian surface compositions from MGS-TES. *Science* 287:1626–1630.

Bandfield J. L. 2004. Identification of quartzofeldspathic materials on Mars. *Journal of Geophysical Research* 109: E10009.

Banerdt W. B., Phillips R. J., Sleep N. H., and Saunders R. S. 1982. Thick shell tectonics on one-plate planets: Applications to Mars. *Journal of Geophysical Research* 87:9723.

Beck P., Barrat J., Chaussidon M., Gillet P., and Bohn M. 2004. Li isotopic variations in single pyroxenes from the Northwest Africa 480 shergottite (NWA 480): A record of degassing of Martian magmas? *Geochimica et Cosmochimica Acta* 68:2925–2933.

Bibring J.-P. and Erard S. 2001. The Martian surface composition. *Space Science Reviews* 96: 293–316.

Bridges J. C. and Warren P. 2006. The SNC meteorites: Basaltic igneous processes on Mars. *Journal of the Geological Society* 163:229–251.

Bridges J. C., Schwenzer S. P., Leveille R., Westall F., Wiens R. C., Mangold N., Bristow T., Edwards P., and Berger G. 2015. Diagenesis and clay mineral formation at Gale Crater, Mars. *Journal of Geophysical Research: Planets* 120:1–19.

Carter J. and Poulet F. 2013. Ancient plutonic processes on Mars inferred from the detection of possible anorthositic terrains. *Nature Geoscience* 6:1008–1012.

Clegg S. M., Sklute E. C., Dyar M. D., Barefield J. E., and Wiens R. C. 2009. Multivariate analysis of remote laser-induced breakdown spectroscopy spectra using partial least squares, principal component analysis, and related techniques. *Spectrochimica Acta Part B: Atomic Spectroscopy* 64:79–88.

Clegg S. M., Wiens R. C., Anderson R. C., Forni O., Frydenvang J., Lasue J., Cousin A., Payré V., Boucher T.,

Dyar M. D., McLennan S. M., Morris R. V., Graff T. G., Mertzman S. A., Ehlmann B. L., Belgacem I., Newsom H. E., Clark B. C., Melikechi N., Mezzacappa A., Mcinroy R. E., Martinez R., Gasda P., Gasnault O., and Maurice S. 2016. Recalibration of the Mars science laboratory ChemCam instrument with an expanded geochemical database. *Spectrochimica Acta Part B: Atomic Spectroscopy* 129:64–85.

Collinet M., Médard E., Charlier B., Vander Auwera J., and Grove T. L. 2015. Melting of the primitive Martian mantle at 0.5–2.2 GPa and the origin of basalts and alkaline rocks on Mars. *Earth and Planetary Science Letters* 427:83–94.

Cousin A., Sautter V., Payré V., Forni O., Mangold N., Gasnault O., Le Deit L., Johnson J., Maurice S., Salvatore M., Wiend R. C., Gasda P., and Rapin W. 2017. Classification of igneous rocks analyzed by ChemCam at Gale crater, Mars. *Icarus*, 288: 265–283.

Cox K. G., Gass I. G., and Mallick D. I. J. 1970. The peralkaline volcanic suite of Aden and Little Aden, South Arabia. *Journal of Petrology* 11:433–462.

Cremers D. and Radziemski L. J. 2006. *Handbook of laser-induced breakdown spectroscopy*. Hoboken, New Jersey: John Wiley & Sons.

Delong S. E. and Hoffman M. A. 1975. Alkali/silica distinction between Hawaiian tholeiites and alkali basalts. *Geological Society of America Bulletin* 86:1101–1108.

Dixon J. E. and Clague D. A. 2001. Volatiles in basaltic glasses from Loihi Seamount, Hawaii: Evidence for a relatively dry plume component. *Journal of Petrology* 42:627–654.

Dreibus G. and Wänke H. 1985. Mars, a volatile-rich planet. *Meteoritics* 20:367–381.

Dunn T. L., McSween H. Y., and Christensen P. R. 2007. Thermal emission spectra of terrestrial alkaline volcanic rocks: Applications to Martian remote sensing. *Journal of Geophysical Research* 112:E05001.

Dyar M. D., Tucker J. M., Humphries S., Clegg S. M., Wiens R. C., and Lane M. D. 2011. Strategies for Mars remote laser-induced breakdown spectroscopy analysis of sulfur in geological samples. *Spectrochimica Acta Part B: Atomic Spectroscopy* 66:39–56.

Filiberto J. and Dasgupta R. 2011. Fe^{2+}–Mg partitioning between olivine and basaltic melts: Applications to genesis of olivine-phyric shergottites and conditions of melting in the Martian interior. *Earth and Planetary Science Letters* 304:527–537.

Filiberto J. and Dasgupta R. 2015. Constraints on the depth and thermal vigor of melting in the Martian mantle. *Journal of Geophysical Research: Planets* 120:109–122.

Filiberto J., Treiman A. H., and Le L. 2008. Crystallization experiments on a Gusev Adirondack basalt composition. *Meteoritics & Planetary Science* 43:1137–1146.

Filiberto J., Gross J., and McCubbin F. M. 2016a. Constraints on the water, chlorine, and fluorine content of the Martian mantle. *Meteoritics & Planetary Science* 51:2023–2035.

Filiberto J., Baratoux D., Beaty D., Breuer D., Farcy B. J., Grott M., Jones J. H., Kiefer W. S., Mane P., McCubbin F. M., and Schwenzer S. P. 2016b. A review of volatiles in the Martian interior. *Meteoritics and Planetary Science* 51:1935–1958.

Floyd P. A., Castillo P. R., and Pringle M. 1991. Tholeiitic and alkalic basalts of the oldest Pacific Ocean crust. *Terra Nova* 3:257–265.

Forni O., Maurice S., Gasnault O., Wiens R. C., Cousin A., Clegg S. M., Sirven J.-B., and Lasue J. 2013. Independent component analysis classification of laser induced breakdown spectroscopy spectra. *Spectrochimica Acta Part B: Atomic Spectroscopy* 86:31–41.

Forni O., Gaft M., Toplis M. J., Clegg S. M., Maurice S., Wiens R. C., Mangold N., Gasnault O., Sautter V., Le Mouélic S., Meslin P.-Y., Nachon M., McInroy R. E., Ollila A., Cousin A., Bridges J. C., Lanza N. L., and Dyar M. D. 2015. First detection of fluorine on Mars: Implications for Gale Crater's geochemistry. *Geophysical Research Letters* 42:1020–1028.

Gale A., Dalton C. A., Langmuir C. H., Su Y., and Schilling J. 2013. The mean composition of ocean ridge basalts. *Geochemistry, Geophysics, Geosystems* 14:489–518.

Gasda P., Delapp D., McInroy R. E., Wiens R. C., Bridges J. C., Edwards P. H., Carlson E., Sautter V., Cousin A., Maurice S., Gasnault O., and Clegg S. M. 2016. Identification of fresh feldspars in Gale Crater using ChemCam (abstract #1604). 47th Lunar and Planetary Science Conference. CD-ROM.

Gellert R., Campbell J. L., and King P. L. 2009. The alpha-particle-X-Ray spectrometer (APXS) for the Mars Science Laboratory (MSL) rover mission (abstract #2364). 40th Lunar and Planetary Science Conference. CD-ROM.

Gross J., Treiman A., Filiberto J., and Herd C. 2011. Primitive olivine-phyric shergottite NWA 5789: Petrography, mineral chemistry, and cooling history imply a magma similar to Yamato-980459. *Meteoritics & Planetary Science* 46:116–133.

Gross J., Filiberto J., Herd C. D. K., Daswani M. M., Schwenzer S. P., and Treiman A. H. 2013. Petrography, mineral chemistry, and crystallization history of olivine-phyric shergottite NWA 6234: A new melt composition. *Meteoritics & Planetary Science* 48:854–871.

Grotzinger J. P. 2013. Analysis of surface materials by the Curiosity Mars rover. *Science* 341:1475.

Grotzinger J. P., Crisp J. A., and Vasavada A. R. 2015. Curiosity's mission of exploration at Gale Crater, Mars. *Elements* 11:19–26.

Grove T. L. and Baker M. B. 1984. Phase equilibrium controls on the tholeiitic versus calc-alkaline differentiation trends. *Journal of Geophysical Research: Solid Earth* 89:3253–3274.

Herd C., Treiman A. H., McKay G. A., and Shearer C. K. 2005. Light lithophile elements in Martian basalts: Evaluating the evidence for magmatic water degassing. *Geochimica et Cosmochimica Acta* 69:2431–2440.

Humayun M., Nemchin A., Zanda B., Hewins R. H., Grange M., Kennedy A., Lorand J.-P., Göpel C., Fieni C., Pont S., and Deldicque D. 2013. Origin and age of the earliest Martian crust from meteorite NWA 7533. *Nature* 503:513–516.

Humphreys E. R. and Niu Y. 2009. On the composition of ocean island basalts (OIB): The effects of lithospheric thickness variation and mantle metasomatism. *Lithos* 112:118–136.

Ikeda Y. 2005. Magmatic inclusions in Martian meteorites. *Antarctic Meteorite Research* 18:170.

Irvine T. N. and Baragar W. R. A. 1971. A guide to the chemical classification of the common volcanic rocks. *Canadian Journal of Earth Sciences* 8:523–548.

Johnson M. C., Anderson A. T., and Rutherford M. J. 1994. Pre-eruptive volatile contents of magmas. In *Volatiles in*

magmas, edited by Carroll M. R. and Holloway J. R. Washington, D.C.: Mineralogical Society of America. pp. 281–330.

Karlsson H., Clayton R., Gibson E., and Mayeda T. 1992. Water in SNC meteorites: Evidence for a Martian hydrosphere. *Science* 255:1409–1411.

Karunatillake S., Squyres S. W., Taylor G. J., Keller J. M., Gasnault O., Evans L. G., Reedy R. C., Starr R., Boynton W. V., Janes D. M., Kerry K. E., Dohm J. M., Sprague A. L., Hahn B. C., and Hamara D. 2006. Composition of northern low-albedo regions of Mars: Insights from the Mars Odyssey gamma ray spectrometer. *Journal of Geophysical Research* 112: E03S05.

Koeppen W. C. and Hamilton V. E. 2008. Global distribution, composition, and abundance of olivine on the surface of Mars from thermal infrared data. *Journal of Geophysical Research* 113:E05001.

Le Deit L., Mangold N., Forni O., Cousin A., Lasue J., Schröder S., Wiens R. C., Sumner D., Fabre C., Stack K. M., Anderson R. B., Blaney D., Clegg S., Dromart G., Fisk M., Gasnault O., Grotzinger J. P., Gupta S., Lanza N., Le Mouélic S., Maurice S., McLennan S. M., Meslin P.-Y., Nachon M., Newsom H., Payré V., Rapin W., Rice M., Sautter V., and Treiman A. H. 2016a. The potassic sedimentary rocks in Gale Crater, Mars, as seen by ChemCam on board Curiosity. *Journal of Geophysical Research: Planets* 121:784–804.

Le Mouélic S., Gasnault O., and Herkenhoff K. E. 2015. The ChemCam remote micro-imager at Gale crater: Review of the first year of operations on Mars. *Icarus* 249:93–107.

Leshin L. and Epstein S. 1996. Hydrogen isotope geochemistry of SNC meteorites. *Geochimica et Cosmochimica Acta* 60:2635–2650.

Mangold N., Forni O., Dromart G., Stack K., Wiens R. C., Gasnault O., Sumner D. Y., Nachon M., Meslin P.-Y., Anderson R. B., Barraclough B., Bell J. F. III, Berger G., Blaney D. L., Bridges J. C., Calef F., Clark B., Clegg S. M., Cousin A., Edgar L., Edgett K., Ehlmann B., Fabre C., Fisk M., Grotzinger J., Gupta S., Herkenhoff K. E., Hurowitz J., Johnson J. R., Kah L. C., Lanza N., Lasue J., Le Mouélic S., Léveillé R., Lewin E., Malin M., McLennan S., Maurice S., Melikechi N., Mezzacappa A., Milliken R., Newsom H., Ollila A., Rowland S. K., Sautter V., and Schmidt m., Schröder S., d'Uston C., Vaniman D., and Williams R. 2015. Chemical variations in Yellowknife Bay formation sedimentary rocks analyzed by ChemCam on board the Curiosity rover on Mars. *Journal of Geophysical Research: Planets* 120:452–482.

Mangold N., Thompson L. M., Forni O., Williams A. J., Fabre C., Le Deit L., Wiens R. C., Williams R., Anderson R. B., Blaney D. L., Calef F., Cousin A., Clegg S. M., Dromart G., Dietrich W. E., Edgett K. S., Fisk M. R., Gasnault O., Gellert R., Grotzinger J. P., Kah L., Le Mouélic S., McLennan S. M., Maurice S., Meslin P.-Y., Newsom H. E., Palucis M. C., Rapin W., Sautter V., Siebach K. L., Stack K., Sumner D., and Yingst A. 2016. Composition of conglomerates analyzed by the Curiosity rover: Implications for Gale Crater crust and sediment sources. *Journal of Geophysical Research: Planets* 121:353–387.

Mangold N., Schmidt M. E., Fisk M., Forni O., McLennan S., Ming D., Sautter V., Sumner D., Williams A., Clegg S., Cousin A., Gasnault O., Gellert R., Grotzinger J., and Wiens R. 2017. Classification scheme for sedimentary and igneous rocks un Gale crater, Mars. *Icarus* 284:1–17.

Maurice S. and Cousin A. 2012. Laser induced breakdown spectroscopy (LIBS) spot size at stand-off distances with ChemCam (abstract #2899). 43rd Lunar and Planetary Science Conference. CD-ROM.

Maurice S., Wiens R. C., Saccoccio M., Barraclough B. L., Gasnault O., Forni O., Mangold N., Baratoux D., Bender S. C., Berger G., Bernardin J., Berthé M., Bridges N., Blaney D., Bouyé M., Caïs P., Clark B., Clegg S., Cousin A., Cremers D., Cros A, DeFlores L., Derycke C., Dingler B., Dromart G., Dubois B., Dupieux M., Durand E., d'Uston L., Fabre C., Faure B., Gaboriaud A., Gharsa T., Herkenhoff K., Kan E., Kirkland L., Kouach D., Lacour J.-L., Langevin Y., Lasue J., Le Mouélic S., Lescure M., Lewin E., Limonadi D., Manhès G., Mauchien P., McKay C., Meslin P.-Y., Michel Y., Miller E., Newsom H. E., Orttner G., Paillet A., Parès L., Parot Y., Pérez R., Pinet P., Poitrasson F., Quertier B., Sallé B., Sotin C., Sautter V., Séran H., Simmonds J. J., Sirven J.-B., Stiglich R., Striebig N., Thocaven J.-J., Toplis M. J., and Vaniman D. 2012. The ChemCam instrument suite on the Mars Science Laboratory (MSL) rover: Science objectives and mast unit description. *Space Science Reviews* 170:95–166.

Maurice S., Clegg S. M., Wiens R. C., Gasnault O., Rapin W., Forni O., Cousin A., Sautter V., Mangold N., Le Deit L., Nachon M., Anderson R. C., Lanza N. L., Fabre C., Payré V., Lasue J., Meslin P.-Y., Léveillé R. J., Barraclough B. L., Beck P., Bender S. C., Berger G., Bridges J. C., Bridges N. T., Dromart G., Dyar M. D., Francis R., Frydenvang J., Gondet B., Ehlmann B. L., Herkenhoff K. E., Johnson J. R., Langevin Y., Madsen M. B., Melikechi N., Lacour J.-L., Le Mouélic S., Lewin E., Newsom H. E., Ollila A. M., Pinet P., Schröder S., Sirven J.-B., Tokar R. L., Toplis M. J., d'Uston C., Vanimanj D. T., and Vasavadap A. R. 2016. ChemCam activities and discoveries during the nominal mission of the Mars Science Laboratory in Gale crater, Mars. *Journal of Analytical Atomic Spectrometry* 31:863–889.

McCubbin F. M., Nekvasil H., Harrington A. D., Elardo S. M., and Lindsley D. H. 2008. Compositional diversity and stratification of the Martian crust: Inferences from crystallization experiments on the picrobasalt Humphrey from Gusev Crater, Mars. *Journal of Geophysical Research* 113:E11013.

McCubbin F. M., Boyce J. W., Srinivasan P., Santos A. R., Elardo S. M., Filiberto J., Steele A. and Shearer C. K. 2016. Heterogeneous distribution of H_2O in the Martian interior: Implications for the abundance of H_2O in depleted and enriched mantle sources. *Meteoritics & Planetary Science* 51:2036–2060.

McLennan S. M. 2003. Large-ion lithophile element fractionation during the early differentiation of Mars and the composition of the Martian primitive mantle. *Meteoritics & Planetary Science* 38:895–904.

McLennan S. M., Anderson R. B., Bell III J. F., Bridges J. C., Calef III F., Campbell J. L., Clark B. C., Clegg S., Conrad P., Cousin A., Des Marais D. J., Dromart G., Dyar M. D., Edgar L. A., Ehlmann B. L., Fabre C., Forni O., Gasnault O., Gellert R., Gordon S., Grant J. A., Grotzinger J. P., Gupta S., Herkenhoff K. E., Hurowitz J. A., King P. L., Le Mouélic S., Leshin L. A., Léveillé R., Lewis K. W., Mangold N., Maurice S., Ming D. W., Morris R. V., Nachon M., Newsom H. E., Ollila A. M., Perrett G. M., Rice M. S., Schmidt M. E., Schwenzer S. P., Stack K., Stolper E. M., Sumner D. Y., Treiman A.H.,

VanBommel S., Vaniman D. T., Vasavada A., Wiens R. C., and Yingst R. A. 2014. Elemental geochemistry of sedimentary rocks in Yellowknife Bay, Gale Crater, Mars. *Science* 343. https://doi.org/10.1126/science.1244734.

McSween H. Y. 2002. The rocks of Mars, from far and near. *Meteoritics & Planetary Science* 37:7–25.

McSween H. Y. and Ruff S. W. 2006. Alkaline volcanic rocks from the Columbia Hills, Gusev crater, Mars. *Journal of Geophysical Research: Planets* 111:1–15.

McSween H. Y. and Treiman A. H. 1998. Martian meteorites. *Reviews in Mineralogy and Geochemistry* 36:1–653.

McSween H. Y., Murchie S. L., Crisp J. A., Bridges N. T., Anderson R. C., Bell J. F., Britt D. T., Brückner J., Dreibus G., Economou T., Ghosh A., Golombek M. P., Greenwood J. P., Johnson J. R., Moore H. J., Morris R. V., Parker T. J., Rieder R., Singer R., and Wänke H. 1999. Chemical, multispectral, and textural constraints on the composition and origin of rocks at the Mars Pathfinder landing site. *Journal of Geophysical Research: Planets* 104:8679–8715.

McSween H. Y., Grove T. L., Lentz R. C., Dann J. C., Holzheid A. H., Riciputi L. R., and Ryan J. G. 2001. Geochemical evidence for magmatic water within Mars from pyroxenes in the Shergotty meteorite. *Nature* 409:487–490.

McSween H. Y., Grove T. L., and Wyatt M. B. 2003. Constraints on the composition and petrogenesis of the Martian crust. *Journal of Geophysical Research: Planets* 108:5135.

McSween H. Y., Ruff S. W., Morris R. V., Gellert R., Klingelhöfer G., Christensen P. R., McCoy T. J., Ghosh A., Moersch J. M., Cohen B. A., Rogers A. D., Schröder C., Squyres S. W., Crisp J., and Yen A. 2008. Mineralogy of volcanic rocks in Gusev Crater, Mars: Reconciling Mössbauer, Alpha Particle X-Ray Spectrometer, and Miniature Thermal Emission Spectrometer spectra. *Journal of Geophysical Research* 113:E06S04.

McSween H. Y., Taylor G. J., and Wyatt M. B. 2009. Elemental composition of the Martian crust. *Science* 324:736–739.

McSween H. Y., Labotka T. C., and Viviano-Beck C. E. 2015. Metamorphism in the Martian crust. *Meteoritics & Planetary Science* 50:590–603.

Mezger K., Debaille V., and Kleine T. 2012. Core formation and mantle differentiation on Mars. *Space Science Reviews* 174:27–48.

Milliken R. E., Grotzinger J. P., and Thomson B. J. 2010. Paleoclimate of Mars as captured by the stratigraphic record in Gale Crater. *Geophysical Research Letters* 37: L04201. doi:10.1029/2009GL041870

Ming D. W., Gellert R., Morris R. V., Arvidson R. E., Brückner J., Clark B. C., Cohen B. A., D'Uston C., Economou T., Fleischer I., Klingelhöfer G., McCoy T. J., Mittlefehldt D. W., Schmidt M. E., Schröder C., Squyres S. W., Tréguier E., Yen A. S., and Zipfel J. 2008. Geochemical properties of rocks and soils in Gusev Crater, Mars: Results of the Alpha Particle X-Ray Spectrometer from Cumberland Ridge to Home Plate. *Journal of Geophysical Research* 113:E12S39.

Morris R. V., Klingelhöfer G., Schröder C., Rodionov D. S., Yen A. S., Ming D. W., De SouzaJr . P. A., Fleischer I., Wdowiak T., Gellert R., Bernhardt B., Evlanov E. N., Zubkov B., Foh J., Bonnes U., Kankeleit E., Gütlich P., Renz F., Squyres S. W., and Arvidson R. E. 2006. Mössbauer mineralogy of rock, soil, and dust at Gusev crater, Mars: Spirit's journey through weakly altered olivine basalt on the plains and pervasively altered basalt in the Columbia Hills. *Journal of Geophysical Research: Planets* 111:E2.

Morris R. V., Vaniman D. T., Blake D. F., Gellert R., Chipera S. J., Ming D. W., Morrison S. M., Downs R. T., Rampe E. B., Treiman A. H., Yen A. S., Achilles C. N., Bristow T. F., Fendrich K., Crisp J. A., Des Marais D. J., Farmer J. D., Grotzinger J. P., Morookian J. M., Stolper E. M., and Schwenzer S. P. 2016. High-temperature, perhaps silicic, volcanism on mars evidenced by tridymite detection in high-SiO_2 sedimentary rock at Gale Crater, Mars. *Icarus* 113:7071–7076. doi: 10.1073/pnas.1607098113

Musselwhite D. S., Dalton H. A., Kiefer W. S., and Treiman A. H. 2005. Experimental petrology of the basaltic shergottite Yamato-980459: Implications for the thermal structure of the Martian mantle. *Meteoritics & Planetary Science Archives* 41:1271–1290.

Nachon M., Clegg S. M., Mangold N., Schröder S., Kah L. C., Dromart G., Ollila A., Johnson J. R., Oehler D. Z., Bridges J. C., Le Mouélic S., Forni O., Wiens R. C., Anderson R. C., Blaney D. L., Bell J. F., Clark B. C., Cousin A., Dyar M. D., Ehlmann B., Fabre C., Gasnault O., Grotzinger J., Lasue J., Lewin E., Léveillé R., McLennan S., Maurice S., Meslin P.-Y., Rapin W., Rice M., Squyres S. W., Stack K., Sumner D. Y., Vaniman D., and Wellington D. 2014. Calcium sulfate veins characterized by ChemCam/Curiosity at Gale crater, Mars. *Journal of Geophysical Research: Planets* 119:1991–2016.

Nekvasil H. 2004. The origin and evolution of silica-saturated alkalic suites: An experimental study. *Journal of Petrology* 45:693–721.

Nekvasil H., Filiberto J., McCubbin F. M., and Lindsley D. H. 2007. Alkalic parental magmas for chassignites? *Meteoritics & Planetary Science* 42:979–992.

Nekvasil H., McCubbin F. M., Harrington A. D., Elardo S. M., and Lindsley D. H. 2009. Linking the Chassigny meteorite and the Martian surface rock Backstay: Insights into igneous crustal differentiation processes on Mars. *Meteoritics & Planetary Science* 44:853–869.

Nicholls I. A. and Ringwood A. E. 1972. Production of silica-saturated tholeiitic magmas in island arcs. *Earth and Planetary Science Letters* 17:243–246.

Nimmo F. and Stevenson D. J. 2001. Estimates of Martian crustal thickness from viscous relaxation of topography. *Journal of Geophysical Research: Planets* 106:5085–5098.

Nyquist L. E., Bogard D. D., Shih C.-Y., Greshake A., Stöffler D., and Eugster O. 2001. Ages and geologic histories of Martian meteorites. In *Chronology and evolution of Mars*, edited by Kallenbach R., Geiss J., and Hartmann W. K. Dordrecht, the Netherlands: Springer. pp. 105–164.

Papike J. J., Burger P. V., Shearer C. K., and McCubbin F. M. 2013. Experimental and crystal chemical study of the basalt–eclogite transition in Mars and implications for Martian magmatism. *Geochimica et Cosmochimica Acta* 104:358–376.

Poulet F., Mangold N., Platevoet B., Bardintzeff J.-M., Sautter V., Mustard J. F., Bibring J.-P., Pinet P., Langevin Y., Gondet B., and Aléon-Toppani A. 2009. Quantitative compositional analysis of Martian mafic regions using the MEx/OMEGA reflectance data. *Icarus* 201:84–101.

Rampe E. B., Ming D. W., Blake D. F., Bristow T. F., Chiperac S. J., Grotzinger J. P., Morris R. V., Morrison S.

M., Vanimang D. T., Yen A. S., Achilles C. N., Craig P. I., Des Marais D. J., Downs R. T., Farmer J. D., Fendrich K. V., Gellert R., Hazen R. M., Kah L. C., Morookian J. M., Peretyazhko T. S., Sarrazin P., Treiman A. H., Bergeo J. A., Eigenbrode J., Fairén A. G., Forni R. O., Gupta S., Hurowitz J. A., Lanza N. L., Schmidt M. E., Siebach K., Sutter B., and Thompson L. M. 2017. Mineralogy of an ancient lacustrine mudstone succession from the Murray formation, Gale crater, Mars. *Earth and Planetary Science Letters* 471:172–185.

Rice M. 2014. Geology of The Kimberley Waypoint, Gale Crater: Observations from orbit and MSL Curiosity. 2014 GSA Annual Meeting 202.

Rogers A. D. and Hamilton V. E. 2015. Compositional provinces of Mars from statistical analyses of TES, GRS, OMEGA and CRISM data. *Journal of Geophysical Research: Planets* 120:62–91.

Saal A. E., Hauri E. H., Langmuir C. H., and Perfit M. 2002. Vapour undersaturation in primitive mid-ocean-ridge basalt and the volatile content of Earth's upper mantle. *Nature* 419:451–455.

Santos A. R., Agee C. B., McCubbin F. M., Shearer C. K., Burger P. V., Tartèse R., and Anand M. 2015. Petrology of igneous clasts in Northwest Africa 7034: Implications for the petrologic diversity of the Martian crust. *Geochimica et Cosmochimica Acta* 157:56–85.

Sautter V., Fabre C., and Forni O. 2014. Igneous mineralogy at Bradbury Rise: The first ChemCam campaign at Gale crater. *Journal of Geophysical Research: Planets* 119:30–46.

Sautter V., Toplis M. J., Wiens R. C., Cousin A., Fabre C., Gasnault O., Maurice S., Forni O., Lasue J., Ollila A., Bridges J. C., Mangold N., Le Mouélic S., Fisk M. R., Meslin P.-Y., Beck P., Pinet P., Le Deit L., Rapin W., Stolper E. M., Newsom H., Dyar D., Lanza N., Vaniman D., Clegg S., and Wray J. J. 2015. In situ evidence for continental crust on early Mars. *Nature Geoscience* 8:605–609.

Schmidt M. E. and McCoy T. J. 2010. The evolution of a heterogeneous Martian mantle: Clues from K, P, Ti, Cr, and Ni variations in Gusev basalts and shergottite meteorites. *Earth and Planetary Science Letters* 296:67–77.

Schmidt M. E., Schrader C. M., and McCoy T. J. 2013. The primary fO_2 of basalts examined by the Spirit rover in Gusev Crater, Mars: Evidence for multiple redox states in the Martian interior. *Earth and Planetary Science Letters* 384:198–208.

Schmidt M. E., Campbell J. L., Gellert R., Perrett G. M., Treiman A. H., Blaney D. L., Olilla A., Calef III F. J., Edgar L., Elliott B. E., Grotzinger J., Hurowitz J., King P. L., Minitti M. E., Sautter V., Stack K., Berger J. A., Bridges J. C., Ehlmann B. L., Forni O., Leshin L. A., Lewis K. W., McLennan S. M., Ming D. W., Newsom H., Pradler I., Squyres S. W., Stolper E. M., Thompson L., VanBommel S., and Wiens R. C. 2014. Geochemical diversity in first rocks examined by the Curiosity Rover in Gale Crater: Evidence for and significance of an alkali and volatile-rich igneous source. *Journal of Geophysical Research: Planets* 119:64–81.

Schroder S., Meslin P.-Y., Gasnault O., Maurice S., Cousin A., Wiens R. C., Rapin W., Dyar M. D., Mangold N., Forni O., Nachon M., Clegg S., Johnson J. R., Lasue J., le Mouelic Ollila A., Pinet P., Sautter V., and Vaniman D. 2015. Hydrogen detection with ChemCam at Gale crater. *Icarus* 249:43–61.

Schwenzer S. P., Bridges J. C., McAdam A., Steer E. D., Conrad P. G., Kelley S. P., Wiens R. C., Mangold N., Grotzinger J. P., Eigenbrode J. L., Franz H. B., and Sutter B. 2016. Modeling of sulphide environments on Mars. *Meteoritics & Planetary Science* 51:2175–2202. doi:10.1111/maps.12668

Shearer C. K., Burger P. V., Papike J. J., Borg L. E., Irving A. J., and Herd C. 2008. Petrogenetic linkages among Martian basalts: Implications based on trace element chemistry of olivine. *Meteoritics & Planetary Science Archives* 43:1241–1258.

Shearer C. K., Aaron P. M., Burger P. V., Guan Y., Bell A. S., and Papike J. J. 2013. Petrogenetic linkages among fO_2, isotopic enrichments-depletions and crystallization history in Martian basalts. Evidence from the distribution of phosphorus in olivine megacrysts. *Geochimica et Cosmochimica Acta* 120:17–38.

Spulber S. D. and Rutherford M. J. 1983. The origin of rhyolite and plagiogranite in oceanic crust: An experimental study. *Journal of Petrology* 24:1–25.

Squyres S. W., Arvidson R. E., Bell J. F., Brückner J., Cabrol N. A., Calvin W., Carr M. H., Christensen P. R., Clark B. C., Crumpler L., Des Marais D. J., D'Uston C., Economou T., Farmer J. D., Farrand W. H., Folkner W., Golombek M. P., Gorevan S., Grant J. A., Greeley R., Grotzinger J., Haskin L., Herkenhoff K. E., Hviid S., Johnson J., Klingelhöfer G., Knoll A., Landis G., Lemmon M., Li R., Madsen M. B., Malin M. C., McLennan S. M., McSween H. Y., Ming D. W., Moersch J., Morris R. V., Parker T., Rice Jr . J. W., Richter L., Rieder R., Sims M., Smith M., Smith P., Soderblom L. A., Sullivan R., Wänke H., Wdowiak T., Wolff M., and Yen A. 2004. The Spirit Rover's Athena science investigation at Gusev Crater, Mars. *Science* 305:794–799.

Squyres S. W., Aharonson O., Clark B. C., Cohen B. A., Crumpler L., De SouzaJr . P. A., Farrand W. H., Gellert R., Grant J. A., Grotzinger J. P., Haldemann A. F. C., Johnson J. R., Klingelhöfer G., Lewis K. W., Li R., McCoy T. J., McEwen A. S., McSween H. Y., Ming D. W., Moore J. M., Morris R. V., Parker T. J., Rice . J. W. Jr., Ruff S., Schmidt M., der Schrö C., and Soderblom L. A. 2007. Pyroclastic activity at Home Plate in Gusev Crater, Mars. *Science* 316:738–742.

Stolper E. M. and McSween H. Y. 1979. Petrology and origin of the shergottite meteorites. *Geochimica et Cosmochimica Acta* 43:1475–1498.

Stolper E. M., Baker M. B., Newcombe M. E., Schmidt M. E., Treiman A. H., Cousin A., Dyar M. D., Fisk M. R., Gellert R., King P. L., Leshin L., Maurice S., McLennan S. M., Minitti M. E., Perrett G., Rowland S., Sautter V., and Wiens R. C. 2013. The petrochemistry of Jake_M: A Martian mugearite. *Science* 341:1239463.

Taylor G. J. 2013. The bulk composition of Mars. *Chemie der Erde—Geochemistry* 73:401–420.

Taylor G. J., Martel L. M. V., Karunatillake S., Gasnault O., and Boynton W. V. 2010. Mapping Mars geochemically. *Geology* 38:183–186.

Taylor S. R., and McLennan S. M. 2009. *Planetary crusts*. New York: Cambridge University Press. p. 382.

Thompson L. M., Schmidt M. E., Perrett G., Elliott B., Gellert R., and Fisk M. 2016. K-Rich Rocks at Gale, Dingo Gap to the Kimberley: An APXS Perspective. Eighth International Conference on Mars.

Treiman A. H. and Filiberto J. 2015. Geochemical diversity of shergottite basalts: Mixing and fractionation, and their relation to Mars surface basalts. *Meteoritics & Planetary Science* 50:632–648.

Treiman A. H., Bish D. L., Vaniman D. T., Chipera S. J., Blake D., Ming D. W., Morris R. V., Bristow T. F., Morrison S. M., Baker M. B., Rampe E. B., Downs R. T., Filiberto J., Glazner A. F., Gellert R., Thompson L., Schmidt M. E., Le Deit L., Wiens R. C., McAdam A. C., Achilles C. N., Edgett K. S., Farmer J. D., Fendrich K. V., Grotzinger J. P., Gupta S., Morookian J. M., Newcombe M. E., Rice M. S., Spray J. G., Stolper E. M., Sumner D. Y., Vasavada A. R., and Yen A. S. 2016. Mineralogy, provenance, and diagenesis of a potassic basaltic sandstone on Mars: CheMin X-ray diffraction of the Windjana sample (Kimberley area, Gale Crater). *Journal of Geophysical Research: Planets* 121:75–106.

Udry A. and Howarth G. H. 2016. Petrogenesis of the enriched shergottite Northwest Africa 7320: A new Martian gabbroic sample (abstract #1704). 47th Lunar and Planetary Science Conference. CD-ROM.

Usui T., McSween H. Y., and Clark B. C. 2008. Petrogenesis of high-phosphorous Wishstone Class rocks in Gusev Crater, Mars. *Journal of Geophysical Research* 113: E12S44.

Usui T., Alexander C. M. O., Wang J., Simon J. I., and Jones J. H. 2012. Origin of water and mantle–crust interactions on Mars inferred from hydrogen isotopes and volatile element abundances of olivine-hosted melt inclusions of primitive shergottites. *Earth and Planetary Science Letters* 357–358:119–129.

Usui T., Alexander C. M. O., Wang J., Simon J. I., and Jones J. H. 2015. Meteoritic evidence for a previously unrecognized hydrogen reservoir on Mars. *Earth and Planetary Science Letters* 410:140–151.

Vaniman D. T., Bish D. L., Ming D. W., Bristow T. F., Morris R. V., Blake D., Christensen P. R., Morrison S. M., Treiman A. H., Rampe E. B., Rice M., Achilles C. N., Grotzinger J. P., McLennan S. M., Williams J., Bell J. F., Newsom H. E., Downs R. T., Maurice S., Sarrazin P., Yen A. S., Morookian J. M., Farmer J. D., Stack K., Milliken R. E., Ehlmann B. L., Sumner D. Y., Berger G., Crisp J. A., Hurowitz J. A., Anderson R., Des Marais D. J., Stolper E. M., Edgett K. S., Gupta S., and Spanovich N. 2014. Mineralogy of a mudstone at Yellowknife Bay, Gale crater, Mars. *Science* 343:1243480.

Whitaker M. L., Nekvasil H., and Lindsley D. H. 2005. Potential magmatic diversity on Mars. 36th Annual Lunar and Planetary Science Conference. CD-ROM.

Whitaker M. L., Nekvasil H., Lindsley D. H., and Difrancesco N. J. 2007. The role of pressure in producing compositional diversity in intraplate basaltic magmas. *Journal of Petrology* 48:365–393.

Wiens R. C. and Maurice S. 2015. ChemCam: Chemostratigraphy by the first Mars microprobe. *Elements* 11:33–38.

Wiens R. C., Maurice S., Barraclough B. L., Saccoccio M., Barkley W. C., Bell J. F., Bender S. C., Bernardin J., Blaney D. L., Blank J., Bouyé M., Bridges N., Bultman N., Caïs P., Clanton R. C., Clark B., Clegg S., Cousin A., Cremers D., Cros A., DeFlores L., Delapp D., Dingler R., D'Uston C., Dyar M. D., Elliott T., Enemark D., Fabre C., Flores M., Forni O., Gasnault O., Hale T., Hays D., Herkenhoff K., Kan E., Kirkland L., Kouach D., Landis D., Langevin Y., Lanza N., LaRocca F., Lasue J., Latino J., Limonadi D., Lindensmith C., Little C., Mangold N., Manhes G., Mauchien P., McKay C., Miller E., Mooney J., Morris R. V., Morrison L., Nelson T., Newsom H., Ollila A., Ott M., Pares L., Perez R., Poitrasson F., Provost C., Reiter J. W., Roberts T., Romero F., Sautter V., Simmonds S. S., Stiglich R., Storms S., Striebig N., Thocaven J.-J., Trujillo T., Ulibarri M., Vaniman D., Warner N., Waterbury R., Whitaker R., Witt J., and Wong-Swanson B. 2012. The ChemCam instrument suite on the Mars Science Laboratory (MSL) rover: Body unit and combined system tests. *Space Science Reviews* 170:167–227.

Wiens R. C., Maurice S., and Lasue J. 2013. Pre-flight calibration and initial data processing for the ChemCam laser-induced breakdown spectroscopy instrument on the Mars Science Laboratory rover. *Spectrochimica Acta Part B: Atomic Spectroscopy* 82:1–27.

Williams R. M. E., Grotzinger J. P., Dietrich W. E., Gupta S., Sumner D. Y., Wiens R. C., Mangold N., Malin M. C., Edgett K. S., Maurice S., Forni O., Gasnault O., Ollila A., Newsom H. E., Dromart G., Palucis M. C., Yingst R. A., Anderson R. C., Herkenhoff K. E., Le Mouélic S., Goetz W., Madsen M. B., Koefoed A., Jensen J. K., Bridges J. C., Schwenzer S. P., Lewis K. W., Stack K. M., Rubin D., Kah L. C., Bell III J. F., Farmer J. D., Sullivan R., Van Beek T., Blaney D. L., Pariser O., Deen R. G., and the MSL Science Team. 2013. Martian fluvial conglomerates at Gale crater. *Science* 340:1068–1072.

Wilson B. M. 2007. *Igneous petrogenesis: A global tectonic approach*. Dordrecht, the Netherlands: Springer Science & Business Media.

Wray J. J., Hansen S. T., Dufek J., Swayze G. A., Murchie S. L., Seelos F. P., Skok J. R., Irwin R. P., and Ghiorso M. S. 2013. Prolonged magmatic activity on Mars inferred from the detection of felsic rocks. *Nature Geoscience* 6:1013–1017.

Yoder H. S. and Tilley C. E. 1962. Origin of basalt magmas: An experimental study of natural and synthetic rock systems. *Journal of Petrology* 3:342–532.

Zimmer M. M., Plank T., Hauri E. H., Yogodzinski G. M., Stelling P., Larsen J., Singer B., Jicha B., Mandeville C., and Nye C. J. 2010. The role of water in generating the calc-alkaline trend: New volatile data for Aleutian magmas and a new tholeiitic index. *Journal of Petrology* 51:2411–2444.

Zipfel J., Schröder C., Jolliff B. L., Gellert R., Herkenhoff K. E., Rieder R., Anderson R. C., Bell J. F., Brückner J., Crisp J. A., Christensen P. R., Clark B. C., De Souza Jr. P. A., Dreibus G., D'uston C., Economou T., Gorevan S., Hahn B. C., Klingelhöfer G., McCoy T. J., McSween H. Y. Jr., Ming D. W., Morris R. V., Rodionov D. S., Squyres S. W., Wänke H., Wright S. P., Wyatt M. B., and Yen A. S. 2011. Bounce Rock—A shergottite-like basalt encountered at Meridiani Planum, Mars. *Meteoritics & Planetary Science* 46:1–20.

SUPPORTING INFORMATION

Additional supporting information may be found in the online version of this article:

Data S1. Basalt–trachybasalt samples from Gale Crater, Mars.

Table S1. Error on each dataset. RMSE for CCAM at the two focal points of data representing accuracy.

Table S2. Shergottite compositions.

Data S2. Reference list.